

Title

Biodegradable and electrically conductive melanin-Poly (3-hydroxybutyrate) 3D fibrous scaffolds for neural tissue engineering applications

Lokesh Agrawal^{1,2#}, Sunil Kumar Vimal^{3,4#*}, Paolo Barzaghi⁵, Shiga Takashi^{2,6}, Marco Terenzio^{1*}

¹Molecular Neuroscience Unit, Okinawa Institute of Science and Technology Graduate University, Kunigami-gun, Okinawa 904-0412, Japan.

²Graduate School of Comprehensive Human Sciences, Kansei, Behavioral and Brain Sciences, University of Tsukuba, 1-1-1 Tennodai, Tsukuba, 305-8577, Japan.

³Department of Pharmaceutical Sciences Southwest University Chongqing 400715, P. R. China.

⁴Universidad Integral del Caribe y América Latina, Kaminda Cas Grandi #79, Willemstad, Curacao.

⁵Scientific imaging section, Okinawa Institute of Science and Technology Graduate University, Kunigami-gun, Okinawa 904-0412, Japan.

⁶Department of Neurobiology, Faculty of Medicine, University of Tsukuba, 1-1-1 Tennodai, Tsukuba, 305-8577, Japan.

These authors contributed equally to this work

* *Corresponding Authors*

This article has been accepted for publication and undergone full peer review but has not been through the copyediting, typesetting, pagination and proofreading process, which may lead to differences between this version and the [Version of Record](#). Please cite this article as [doi: 10.1002/mabi.202200315](https://doi.org/10.1002/mabi.202200315).

This article is protected by copyright. All rights reserved.

- *Sunil Kumar Vimal, Assistant Professor, Traditional medicines, Universidad Integral del Caribe y América Latina, Kaminda Cas Grandi #79, Willemstad, Curacao; Email: sunilkvimal@unical.university*
- *Marco Terenzio, Assistant Professor, Molecular Neuroscience Unit, OIST, Japan; Email: marco.terenzio@oist.jp*

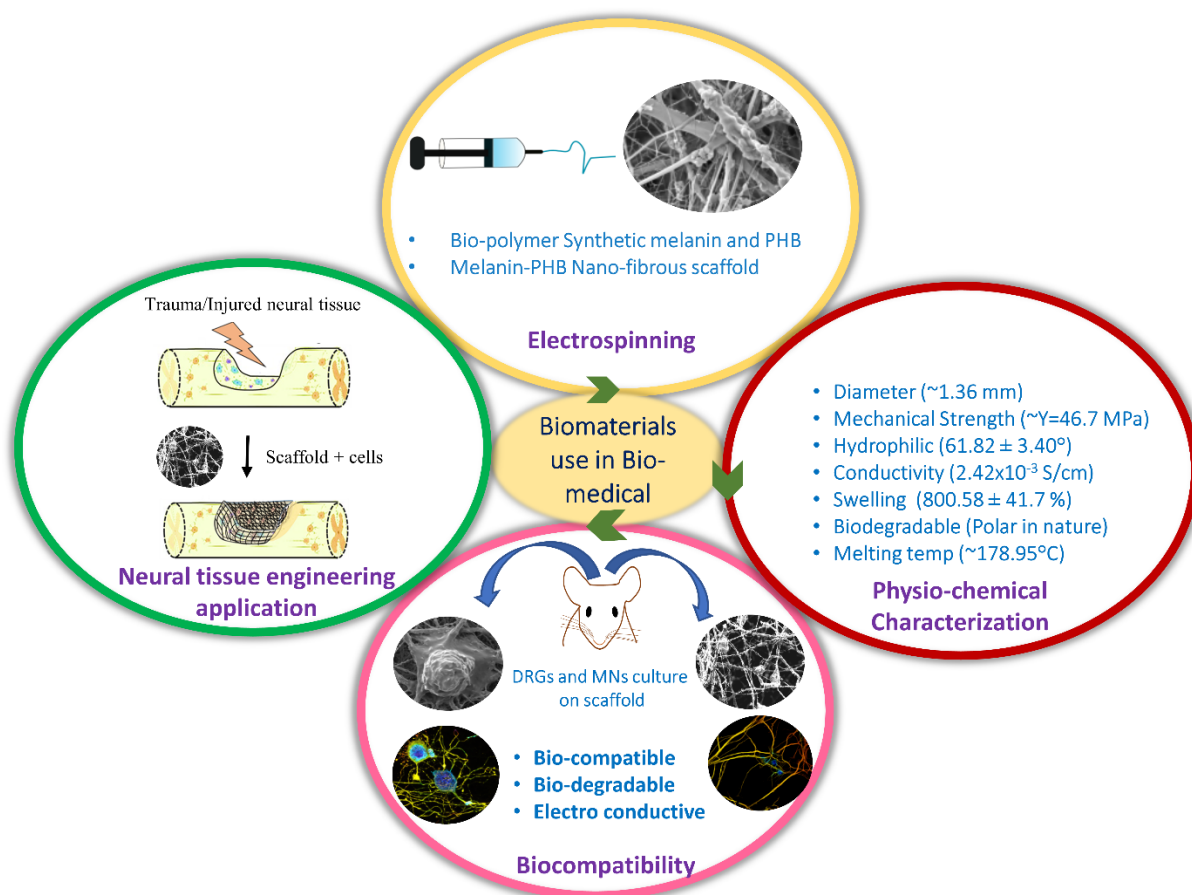
Keywords

Electrospinning, fibrous scaffolds, electroconductive, biodegradable, melanin, Poly (3-hydroxybutyrate), neural tissue engineering

Abstract

Due to the severity of peripheral nerve and spinal cord injuries, treatment options for patients are limited. In this context, biomaterials designed to promote regeneration and reinstate the lost function are being explored. Such biomaterials should be able to mimic the biological, chemical, and physical cues of the extracellular matrix for maximum effectiveness as therapeutic agents. Development of biomaterials with desirable physical, chemical, and electrical properties, however, has proven challenging. Here, we propose a novel biomaterial formulation achieved by blending the pigment melanin and the natural polymer Poly (3-hydroxybutyrate). Physio-chemical measurements of electrospun fibers revealed a feature rich surface nano-topography, a semiconducting-nature and brain-tissue-like poroviscoelastic properties. Resulting fibers improved cell adhesion and growth of mouse sensory and motor neurons, without any observable toxicity. Further, the presence of polar functional groups positively affected the kinetics of fibers degradation at a pH (~7.4) comparable to that of body fluids. Thus, melanin-PHB blended scaffolds were found to be physio-chemically, electrically, and biologically compatible with neural tissues and could be used as a regenerative modality for neural tissue injuries.

Table of Content



We developed a biomaterial for scaffolds intended to promote regeneration of nerve tissue after injury. This biomaterial, obtained by mixing the pigment melanin and the natural polymer Poly-3-hydroxybutyrate (PHB), is biodegradable, electrically conductive, and beneficial to the growth of motor and sensory neurons. Thus, we believe this biomaterial can be used in the context of health care applications.

1. Introduction

The development of biomaterials with suitable mechanical strength, biocompatibility, electrical conductivity, and biodegradability, is a critical step for the use of biomedical scaffolds in the healthcare sector. Indeed, nanofiber scaffolds, characterized by a mechanically stable continuous surface with interconnected pores, are uniquely positioned to be used as a matrix to fill the gap left by injury and support the regrowth of damaged neural tissues [1]–[4]. In addition, 3D-scaffolds/hydrogels in combination with microfluidic chips are being investigated to develop *in vitro* models for brain proxies/ organoids as an alternative to animal models [5], [6]. In recent years, various biomaterials have been tested in nerve, cardiac, and bone tissue engineering [7], and shown to improve the structural integrity of the regenerating tissue after nerve injury [7]–[10]. Indeed, by mimicking the natural architecture of the extracellular matrix (ECM), scaffolds promote cell adhesion, proliferation, and differentiation through the interaction between the scaffold fibers and the regenerating cells [11], [12]. For these reasons, conventional and leading-edge scaffold technologies are being tested to address patient's needs in the healthcare system [2], [4], [12], [13], but development of biomaterials approximating the poroviscoelastic and conducting properties of brain-tissue, while also being biodegradable, has proven to be challenging [7], [10], [14], [15]. Indeed, brain's electrical, mechanical and physiological cues, act as critical signals regulating proliferation, migration, and differentiation of neural stem cells [16]–[18]. Therefore, an ideal scaffold should replicate the electrical and mechanical features of the brain-tissue [14].

Currently, electrospinning, photolithography, 3D-printing or 3D-bioprinting can be used to fabricate precisely textured fibrous scaffolds, micro-patterned thin films, and implantable grafts composed of natural or synthetic polymers. These scaffolds can be used for neural tissue engineering (NTE) applications alone or in combination with cells [19]–[22]. Electrospinning is a simple and inexpensive technology that has been successfully employed for the generation of nano/micro-fibrous scaffolds. The resulting fibrous scaffolds are generally non-conducting and thus not suitable to provide electrical stimuli (ES) to nerve cells growing on these surfaces [17]. Indeed, electrically conducting polymers (ECP) are not easy to fabricate through electrospinning [14], [15]. A

possible solution is represented by blending ECPs with suitable biocompatible polymers to create composite fibers [23], [24]. We previously explored the role of electro-spun aligned fibers and 2-photon lithography in the directed growth of axons [4], [19]. In this study, we propose to design a new biomaterial by blending ECP with natural polymers, which is compatible with electrospinning and allows for the construction of biodegradable fibrous scaffolds. Thus, we blended Poly (3-hydroxybutyrate) (PHB), which has already been explored as an implant material to guide axonal growth after nerve injury [25], and melanin, a natural electroactive pigment with antimicrobial and antioxidant properties [16], [21]-[25]. Furthermore, intramuscular melanin injection was shown to promote axon regeneration and improve motor function after sciatic nerve injury in rats [30], making it an ideal candidate for nerve regeneration.

While biodegradable and conductive melanin-based composite thin films have been studied, melanin-based fibrous scaffolds and hydrogels have not yet been explored [15], [23], [29], [31], [32]. Thus, we aimed to engineer melanin-PHB composite fibrous scaffolds and characterize their physicochemical and biological properties, such as surface morphology, thermal, mechanical, and chemical properties, hydrophilicity, conductivity, biocompatibility and biodegradability, to assess their suitability for soft tissue engineering applications [3], [8].

We found that blended fibrous scaffolds offered larger area and rougher surface compared to PHB fibers. In addition, we cultured mouse dorsal root ganglia (DRG) and motor neurons (MNs) on fibrous scaffolds, as these neuronal types are typically affected in peripheral nerve and spinal cord injuries [26], [27] [28]. Survival and morphological features of neurons growing on PHB and melanin-PHB fibrous scaffolds were evaluated. Neurons exhibited the same level of survival on all the surfaces tested, including glass coverslips, which are commonly used as substrate for these cultures. Interestingly, DRG neurons displayed greater surface attachment on melanin-PHB fibers, resulting in an enlargement of their somatic area compared to other substrates. Our observations suggest that melanin-PHB electrically conductive and biodegradable 3D-scaffolds promote the growth of sensory and motor neurons. Thus, we believe that our melanin-PHB blend has potential as a biomaterial to be used in NTE applications targeted to the healthcare industry.

2. Materials and methods

2.1. Ethics statement

All experiments were performed following the guidelines of the Okinawa Institute of Science and Technology Graduate University (OIST) genetic manipulation procedures. All animal experiments were performed in accordance with the regulations of OIST animal care and use committee (protocol #2021-326). OIST animal facilities and animal care and use program are accredited by AAALAC International (Ref. #1551).

2.2. Reagents and antibodies

Synthetic Melanin (Sigma M8631), Poly [(R)-3-hydroxybutyric acid (Sigma 363502), Chloroform, 1, 2-dichloroethane and 1, 1, 1, 3, 3, 3-Hexafluoro-2-propanol were purchased from Sigma-Aldrich, St. Louis, USA. SYLGARD™ 184 silicon elastomer kit (Dow chemical company, USA) was used to prepare cured PDMS rings for cell culture. Suppliers for tissue culture media and supplements are individually specified in the method section. Anti- β III tubulin antibody was purchased from GeneTex (#GTX631830) and AlexaFluor 594 anti-mouse secondary antibody from Invitrogen (ThermoFisher Scientific, Japan).

2.3. Fabrication of PHB and melanin-PHB nanofibers

Electrospinning was used to fabricate PHB and melanin blended PHB nanofibers. Processing and operating parameters like polymer concentration, solvent, solvent ratio, mixing time, electrospinning distance, flow rate, applied voltage, needle gauge and also environmental factors (temperature, humidity), which are critical for electrospinning [19] were considered and optimized as follows. PHB was prepared in chloroform and dichloroethane (9% w/v) by mild heating in a hot water bath, and the resulting clear solution was additionally stirred for 4-5h at RT. Separately, a polymeric solution of melanin (4% w/v) was prepared in hexafluoro 2 propanol (HFIP) and dimethyl sulfoxide (DMSO), subsequently added to the prepared PHB solution and further kept for overnight stirring condition at RT (**Table S1**). The homogenously mixed polymer solution was loaded in a glass syringe fitted with a 22-gauge flat tip needle to prevent point discharge effects. The polymer

solution was drawn using a syringe pump at a rate of 0.8 ml/h, under high-electric potential (18 kV). The distance between the tip of the needle and the grounded collector was set to 18 cm. The temperature of $25\pm 2^\circ\text{C}$ and relative humidity (%) of the spinning chamber were kept constant ($\sim 50\%$) during electrospinning. Samples were collected on an aluminum foil and stored in a vacuum desiccator to remove the residual solvents.

2.4 Characterization of PHB and melanin-PHB fibrous scaffolds

2.4.1 Ultrastructure and diameter

Appearance, surface nanotopography, diameter and density of electrospun PHB and melanin-PHB fibers were evaluated using scanning helium ion microscopy (SHIM; ORION Plus) and scanning electron microscopy (SEM; JEOL JSM-7900F) as previously described [4], [19]. Briefly, scaffolds were lyophilized and mounted onto a conducting carbon tape attached to a copper stub. Samples were sputter coated with gold for 3 min followed by analysis under SHIM at a working distance of 9-10 mm, acceleration voltage of 30 kV, and a field of view of 5 μm . SEM micrographs were captured at a working distance of 10 mm and an accelerating voltage of 5 kV at 1000X and 5000X magnifications. Mean fiber diameters were determined from SEM images using ImageJ software.

2.4.2 Chemical composition of PHB and melanin-PHB fibers

To determine the presence of functional groups and the primary and secondary structure of PHB and melanin in electrospun fibers and to confirm melanin's mixability with PHB polymer in the blended fibers, we performed Fourier-transform infrared (FTIR) spectroscopy and X-ray photoelectron spectroscopy (XPS). FTIR spectroscopy (Vertex 80v; Bruker) was done in transmission mode over a range of $400 - 4000 \text{ cm}^{-1}$ (MIR range) at a resolution of $2 \text{ cm}/4 \text{ cm}^{-1}$ with a scan time of 64 and the data was plotted as percentage of transmittance against wave number (cm^{-1}). Elemental composition analysis (carbon, oxygen and nitrogen) was performed using XPS (PHI Quantera SXM ULVAC-PHI) on a KRATOS Axis Ultra HAS and the resulting data was plotted as counts per second (C/S) vs binding energy (eV) [33]. Briefly, ULVAC-PHI instrument was used with Al $K\alpha$ mono X-ray

with laser spot (ϕ) 200 μm of 50 W (15 kV, 3.3 mA) intensity. The take-off angle was kept at 45 degrees. The survey spectra pass energy was 280 eV and the energy step was 0.5 eV. Spectra pass energy and energy step value of 55 eV and 0.1 eV respectively were used for high-resolution acquisition. The atomic concentrations were calculated using the survey scan on aluminum substrate. Poly-hydroxybutyrate was used as a reference sample.

Tracing of the elemental composition of PHB and melanin-PHB fibers using SEM-EDX was also performed to confirm successful blending of melanin and PHB and map the distribution of melanin in blended fibers [34], [35]. Briefly, scaffolds were sputter coated with Osmium (Os) for 2 min and visualized using a scanning electron microscope (SEM; JEOL JSM-7900F), equipped with a front and rear Oxford energy-dispersive X-ray (EDX) detector (Oxford Instruments, UK). SEM micrographs were captured at a working distance of 10 mm and an accelerating voltage of 10 kV at 500x. Aztec-SEM 6.0 (Oxford Instruments, UK) software was used to map the distribution of C, O and N elements in PHB and blended melanin-PHB (9% PHB- 4% melanin) fibers.

2.4.3 Mechanical characterization

Topographic imaging and nanoindentation of nanofibers (dry condition) were analyzed using atomic force microscopy (AFM) images of PHB and melanin-PHB scaffolds. Briefly, images of the scaffolds were acquired using a MultiMode 8 Atomic Force Microscope with a NanoScope V controller and E scanner (Bruker) as previously described [4]. Mechanical characterization was performed using a Peak Force Tapping mode with a RTESPA-150 probe (Bruker) with a nominal spring constant of 5 N/m, nominal frequency of 150 kHz and a nominal tip radius of 8 nm [12]. Scaffolds were studied in air over an area of $5 \times 5 \mu\text{m}^2$ to determine force-displacement curves. The reduced Young's Modulus/DMT modulus was calculated by fitting the retract curve using the Derjaguin, Muller, Toropov (DMT) model [36]. Images were obtained at a scan rate of 1 Hz, a scan size of $5.08 \mu\text{m}$ and a 128×128 pixels resolution. Raw Young's modulus AFM images were processed using the NanoScope Analysis v.1.10 software (Bruker).

Mechanical properties of the dry electrospun PHB and melanin-PHB nanofibers were analyzed using a mechanical analyzer (Bose Electro Force, USA). Dynamic force was applied to the fibers of the

sheet (10 × 10 mm, n=3) and sample's response was measured in terms of length deformation until occurrence of fracture. Mechanical parameters, stress and strain were calculated using the following equations (1) and (2).

$$\text{Stress (Pa)} = \frac{\text{Force (N)}}{\text{Area (m}^2\text{)}} \quad (1)$$

$$\text{Strain} = \frac{\text{Deformation (m)}}{\text{Initial length (m)}} \quad (2)$$

Young's modulus (Y), tensile strength, and (%) elongation, were also calculated based on the stress–strain curve of each sample (**Figure S1A**) [37], [38]. Young's modulus was calculated by measuring the slope within the elastic region of the stress-strain curve, tensile strength was measured from the ultimate stress of the stress-strain curve and elongation was quantified by the value of strain at fracture point [37], [38]. Our methodology is further illustrated in **Figure S1B**.

2.4.4 Thermal properties

The thermal properties of PHB and melanin-PHB scaffolds were characterized using a differential scanning calorimeter (DSC 8500, PerkinElmer) [4]. Samples of the fibers' scaffold were placed in alumina pans, while empty pans were used as a reference. All samples were first heated at a range of 40-250°C at a heating rate of 10°C min⁻¹ under a continuous dry nitrogen flow of 20 mL min⁻¹. Afterwards, the samples were cooled to 40° C at 10°C min⁻¹. After each test, the crystallization/melting peak region from the thermograph was analyzed to determine the crystallization (Tc)/melting (Tm) points.

2.4.5 Conductivity measurement

2-probes and 4-probes methods are generally used to measure the resistivity (conductivity) of a material, including fibers [39]. The electrical resistivity (or conductivity) of fibers can be measured by using the probe resistance. Briefly, a uniform current density was applied across the specimen sandwiched between two electrodes located on parallel faces. The potential drop across electrodes was then measured. First, we directly measured the resistivity/conductivity of both PHB and melanin-PHB electrospun scaffolds (dry) of known geometry ($1\text{ cm} \times 1\text{ cm} \times 14\ \mu\text{m}$) using a 2-probe method (Cascade Microtech SUMMIT 12000B-AP).

We then confirmed the conductivity of melanin-PHB fibrous scaffold inferring the sheet resistance (R_s) by calculating the slope ($\Delta V/\Delta I$) of the voltage vs current (V/I) curve and multiplying it for the geometric correction factor ($\pi/\ln(2)=4.53236$) as shown in equation (3) [40].

$$R_s = \frac{\pi}{\ln(2)} \left(\frac{\Delta V}{\Delta I} \right) = 4.53236 * \left(\frac{\Delta V}{\Delta I} \right) \quad (3)$$

A geometric correction factor ($\frac{\pi}{\ln(2)}$) was required to account for the limitation of current pathways through the sample, and is based on the sample size, shape and thickness and the position of the probes [40]. If the thickness of the sheet (tf) is known, the sheet resistance (ρ) can be calculated by its resistivity using equation (4) [40]. Conductivity (σ) of fibrous sheets can be calculated by the inverse of resistivity ($1/\rho$).

$$R_s = \frac{\rho}{tf} \quad (4)$$

2.4.6 Hydrophilicity/wettability

Hydrophilicity was determined by observing the contact angle of a water droplet on the scaffolds using a sessile drop method in a contact angle goniometer (KRUSS, GmbH) [4]. Briefly, a water

droplet was poured on the surface of PHB and melanin-PHB samples and the contact angle was measured by Drop Shape Analysis (DSA) software (KRUSS, GmbH).

2.4.6 Swelling and degradation analysis

Swelling and degradation of PHB and melanin-PHB electrospun fibers were estimated *in-vitro* in phosphate buffered saline (PBS, pH 7.4) [41]–[43]. Briefly, dried scaffolds were precisely cut in square shapes (1 cm x 1 cm) and the initial weight was measured. To calculate the degree of swelling both samples were then immersed in 1 ml of PBS (pH 7.4) at 37 °C for 24h, and subsequently weighed. AFM micrographs were also taken to visually confirm the swelling of fibers [42]. For the degradation analysis, after 120 days the scaffolds were rinsed in distilled water, dried in an oven for 24h and weighted. SEM observation was also performed to confirm morphological changes after degradation over a period of 120 days [44]. For the calculation of the degree of swelling (%) and degraded mass (%), we considered the initial dry weight of the scaffold (m_i), the weight of the swelled nanofibers after removing excess water and surface moisture with a filter paper (m_s), and the constant residual weight of the scaffolds after degradation (m_x). The degree of swelling and degraded mass (%) of the scaffolds were calculated from equation (5) and (6).

$$\text{Degree of swelling} = (m_s - m_x / m_x) * 100 \quad (5)$$

$$\text{Degraded mass (\%)} = (m_i - m_x / m_i) * 100 \quad (6)$$

2.5 Cell culture

2.5.1 Preparation for culture

We used 24 well plates for primary neuronal cultures. Scaffolds were placed inside the wells and a Polydimethylsiloxane (PDMS) ring was applied on top of the fiber mesh to prevent it from floating in the medium. For the fabrication of PDMS rings, molds were designed in CAD Rhinoceros3D (V.5, Robert McNeel & Associates) and 3D printed (Object 500 Connex 3, Stratasys, USA) as previously

described [12]. PDMS pre-polymer and catalyst were then mixed thoroughly with a 10:1 ratio in a disposable plastic cup. The mixture was degassed in a vacuum desiccator for 20 min and poured inside the molds. The PDMS was cured in an oven at 60°C for 3h. Finally, polymerized PDMS rings were extracted from the molds and inserted inside the well on top of the scaffolds.

2.5.2 Culture of primary sensory neuron from dorsal root ganglion (DRG)

Scaffolds were placed inside a well of a 24-well plate while being gently pressed down with PDMS rings. Control glass surface and the scaffolds were sterilized with a graded series of ethanol (EtOH) and finally immersed in 99.99% EtOH for 5 min and subsequently washed three times with PBS (each time for 5 min). The samples were then coated with 0.01% Poly-L-lysine (Sigma-Aldrich #P4832-50ml) overnight at 4°C, rinsed with PBS and coated again with Laminin (GibcoBRL #23017-015) for 2h at 4°C. Dorsal Root Ganglia (DRG) neurons were obtained from 2 months old ICR female mice (Charles River or JapanClea, Japan) as described here [45]. Briefly, DRGs were dissected out from adult mice and collected in HBSS (GibcoBRL, #14175095), supplemented with 5 mM HEPES (Sigma-Aldrich, #H0887), and 0.1 mg/ml Primocin (Tamar #ant-pm-1), pH 7.35. Dissociation was performed by digestion with 100 U of papain (Sigma Aldrich, #P4762) in HBSS for 30 min, followed by digestion in 1 mg/ml collagenase-II (Worthington Biochemical Corporation, #CLS2) and 1.2 mg/ml dispase at 37°C in HBSS for 30 min. The ganglia were then triturated in complete HBSS. Cells were recovered by centrifugation in 20% Percoll (Sigma-Aldrich, #P4937) diluted in L15 medium (GibcoBRL #L-5520), with 5 mM HEPES, 10% Fetal Calf Serum (Invitrogen, #10270106), 0.1 mg/ml Primocin, at the speed of 1000 rpm for 8 min and plated at a density of 2×10^4 cells/cm² in F12 medium (GibcoBRL, #11765062) supplemented with 10% Fetal Calf Serum, and 0.1 mg/ml Primocin for 48 hours.

2.5.3 Embryonic motor neurons culture (MNs)

C57/BL6 mouse embryonic stem cells (mESC, #SCRC-1002, ATCC, USA) were cultured and maintained as previously described [4]. Briefly, mESCs were maintained on gelatin coated flasks (EmbryoMax 0.1% Gelatin solution, Merck, #ES-006-B) in Glasgow Minimal Essential Medium (GMEM, Invitrogen #11710035), 5% ES cell-qualified fetal bovine serum (FBS,

Invitrogen, #16141079), 5% knockout serum replacement (KSR, Invitrogen Corporation, #10828028), 1% GLUTAMAX (Invitrogen, #35050061), 0.1 mM 2-mercaptoethanol and 1000 units/ml of leukemia inhibitory factor (Chemicon International, Inc., #ESG1107). To generate MNs, 1.5×10^6 mESC were grown in suspension on a 10 cm non-tissue culture treated Petri dish in presence of differentiation medium (DFNK, 45% Neurobasal (ThermoFisher, #21103049), 45% DMEM/Ham's-F12 (FUJIFILM Wako #041-29775/Invitrogen #11765062), 10% KSR, 1% GLUTAMAX and 0.1 mM 2-mercaptoethanol). 24h after plating, the resulting embryoid bodies (EBs) were centrifuged and re-suspended in 10 ml of DFNK medium. The day after, EBs were allowed to sediment and re-suspended in fresh DFNK medium supplemented with 1 μ M all-trans retinoic acid (RA, Sigma, #R2625) and 333 nM Smoothened Agonist (SAG; Merck, #566660) and maintained as such for additional 4 days. Finally, EBs were dissociated with trypsin-EDTA (Sigma, #T4049) for 7 min at 37°C as previously described [4], [46]. Before seeding, control glass surface and the scaffolds were sterilized with 99.99% EtOH for 5 min and subsequently washed three times with PBS (each time for 5 min). Surfaces were then coated with 0.01% Poly-L-lysine overnight at 4°C, rinsed with PBS and coated again with Laminin for 2h at 4°C. Dissociated motor neurons were plated onto the scaffold in motor neuron growth medium, comprised of Neurobasal medium (ThermoFisher, #21103049) supplemented with 2% B27 (ThermoFisher, #12587010), 2% FBS, 1% GLUTAMAX, 25 μ M 2-mercaptoethanol, 10 ng/ml rat ciliary neurotrophic factor (CNTF; Peprotech, #450-13), 100 pg/ml rat glial cell line-derived neurotrophic factor (GDNF; Peprotech, #450-10) and 1 μ M RA for 48h.

2.6 Immunocytochemistry

Mouse sensory and motor neurons were cultured on PHB and melanin-PHB fibrous scaffolds for 48h and fixed with 4% paraformaldehyde (Electron Microscopy Sciences, #15710) in phosphate buffer saline (PBS, e-Nacalai, #14249-95) for 30 min at room temperature. Blocking for non-specific

antibody binding was performed by incubation with 5% normal goat serum and 0.1% Triton X-100 in PBS for 30 min. Neurons were then incubated overnight at 4°C with anti- β III-tubulin antibody (GeneTex, 1:1000 dilution in PBS), which is a neuronal marker [47]–[49]. Cells were then washed 3-times with PBS and incubated with anti-mouse Alexa Fluor 488 (Invitrogen) conjugated secondary antibody (1:500 dilutions in PBS) for 1h at RT. Imaging for DRG neurons was performed on a confocal laser microscope LSM900 (Carl Zeiss AG, Germany) using 20x (Plan-Apochromat, NA=0.8) and 63x (Plan-Apochromat, NA = 1.40) objective lenses. Images were acquired in ZenBlue 3.1 (Carl Zeiss AG, Germany) with a pixel resolution of 512 x 512 at 20x (0.624 μ m/pixel) and 2048 x 2048 at 63x (0.050 μ m/pixel) for the DRG neurons. Higher resolution images of motor neurons within the scaffold have been acquired on a Nikon-A1R laser confocal microscope (Nikon, Japan) using a PlanApo VC 20x/0.75 NA objective (pixel size = 0.21 μ m).

2.7 Cell viability assay and cell body area estimation

Survival analysis of DRG neurons grown on melanin-PHB and PHB scaffolds was performed to assess the biocompatibility of the material. 1 cm x 1 cm x 10 μ m (LxWxH) fibrous sheets were prepared using electrospinning. DRG neurons were dissociated and cultured for 48h, and cell viability was determined using the CytoPainter Fixable Cell Viability Assay Kit (Fluorometric-Red; ab176744) as previously reported [12]. The fluorescent dye provided in the kit reacts with cell surface amines in alive cells, while necrotic cells display a strong labelling (~500 fold higher than alive cells) of intracellular amines. Indeed, sensitivity of most fluorescent methods for detecting viable cell is higher [50], [51] and exhibit lesser cytotoxicity than conventional methods such as the MTT-assay [52]–[54]. Briefly, cells were incubated with Fluorometric-Red at 37°C for 45 min, washed with HBSS and fixed with 4% paraformaldehyde (Electron Microscopy Sciences, #15710) for 20 min. Cells were then stained with anti- β III-tubulin antibody and Alexa-488 conjugated fluorescent secondary antibody. Fluorescence imaging was performed on a confocal laser scanning microscope LSM900 (Carl Zeiss AG, Germany) using 20x objective as explained in earlier **section-2.6**, and the number of dead (Fluorometric-Red positive cells) and alive cells was counted to estimate cell viability on the different substrates. The same images were then used to quantify the surface area of the cell bodies

of neurons grown on glass surfaces, PHB and melanin-PHB fibers. The software ImageJ was used to manually identify the cell body using a segmented line tool and the area in pixel was calculated for each neuron and later converted to μm^2 .

2.8 SEM imaging of sensory and motor neurons

The morphology of DRG sensory and embryonic motor neurons cultured on glass, PHB and melanin-PHB fibers was qualitatively evaluated by scanning electron microscope (SEM) as reported in our previous work [12]. Briefly, cultured neurons were fixed with 2.5% glutaraldehyde for 20 min. Cells were washed 3 times with PBS (e-Nacalai, #14249-95) for 1 min and fixed with 1% Osmium tetroxide for 20 min. Cells were then washed 5 times with PBS for 5 min and gradually dehydrated using 70%, 90%, and 100% EtOH for 15 min. Samples were treated with t-butyl alcohol (Sigma-Aldrich #471712) before freezing at -30°C for 5 min. Frozen samples were kept inside the Freeze Dryer (ES-2030) at -20°C under vacuum and dried overnight. Dried samples were coated with gold using a multifunction vacuum sputter deposition equipment for 3 min at 0.001 Pa. SEM images were acquired with a JEOL JSM-7900F at 5 KV and 10 mA current with LED detector at magnifications ranging from 900x to 2000x.

2.9 Statistical analysis

ANOVA with Tukey's post hoc test was performed for multiple comparisons and unpaired t-test was performed for the comparison between 2 groups using GraphPad Prism 9 Software (GraphPad, U.S.A.). All the data were expressed as mean \pm SEM, where the error bar indicates the standard error of the mean. * = $P < 0.05$, ** = $P < 0.01$, *** = $P < 0.001$, and **** = $P < 0.0001$.

3 Results

3.1. Morphological characterization of electrospun scaffolds

We aimed to use electrospinning to fabricate PHB and melanin-PHB nanofibers. Synthetic melanin by itself is not a good candidate for spinning due to poor solubility, low plasticity, and brittle nature. Therefore, synthetic melanin was blended with PHB to assist electrospinning and obtain electrically conducting and biodegradable nanofibers (**Table S1**). Successful electrospinning of PHB and melanin-PHB fibrous meshes was validated by SEM imaging. Both PHB and melanin-PHB fibrous sheets were characterized by continuous fibers of random orientations with interconnected pores. PHB fibers displayed a smooth surface, while the surface of melanin-PHB fibers was rough and feature rich (**Figure 1A & 1B**). Fiber diameter (mean \pm s.e.m.) was estimated using images of 5kx magnification. Blending of melanin with PHB resulted in smaller fibers, with PHB and melanin-PHB fibers displaying a diameter of $2.22 \pm 0.055 \mu\text{m}$ and $1.36 \pm 0.0527 \mu\text{m}$ respectively (**Figure 1C, Table 1**). Scanning helium ion microscopy (SHIM) images, which allow for a better visualization of the fiber ultrastructure, also revealed the presence of flakes or nanoparticles-like structures on the surface of melanin-PHB fibers (**Figure 1Bi**). The presence of a mixture of micro and nanofibers (diameter $\sim 0.2\text{-}1 \mu\text{m}$) in melanin-PHB sheets might be the result of the electro-conductive nature of melanin. We expect the mixed diameter of melanin-PHB fibers in conjunction with their rough surface to positively affect the adhesion of nerve cells, by increasing the point of contact of the cells with the scaffold and offering a capillary network for the extension of neurites.

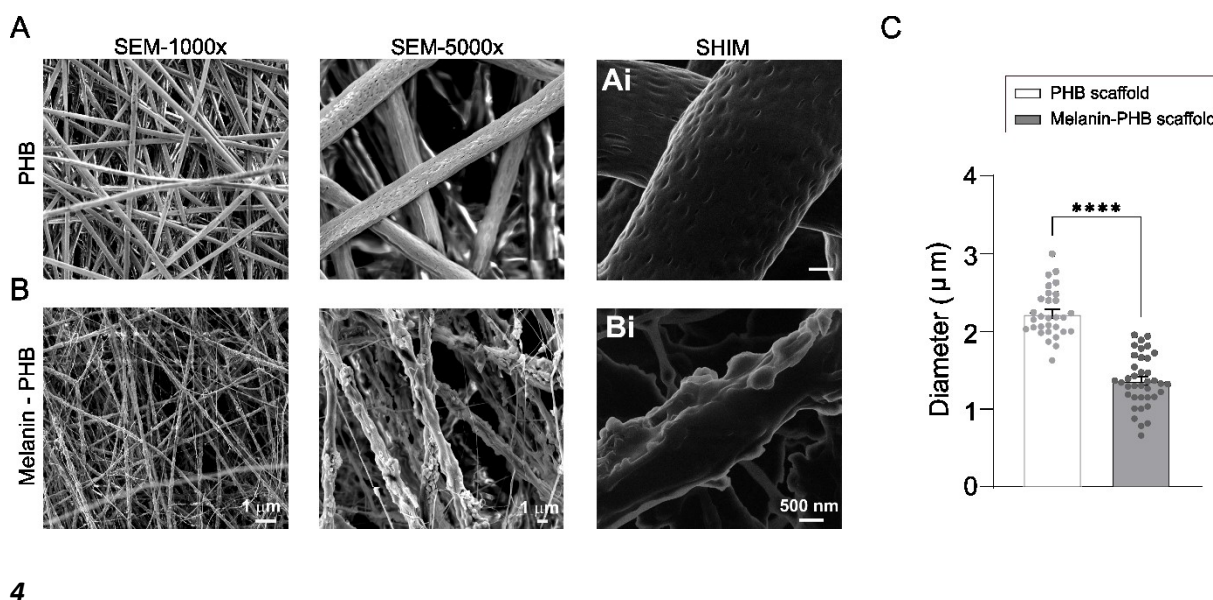


Figure 1: Surface characterization of PHB and melanin-PHB fibers. High resolution SEM images at 1000x and 5000x magnification. (A) PHB scaffold, (B) melanin and PHB composite fibers, and SHIM images showing the ultrastructure and the surface morphology of (Ai) PHB fibers, and (Bi) melanin-PHB fibers. Scale bars: (A-B) at 1000x and 5000x: 1 μm , and (Ai-Bi) 500 nm (C) Quantification of fiber diameter of PHB and melanin-PHB scaffold at 5000x. Data shown as mean \pm s.e.m.; asterisks indicate statistical significance (Student t-test; **** $p \leq 0.0001$).

Measurement	Numeric Values	
	PHB scaffold	Melanin-PHB scaffold
Morphological analysis:		
Fiber diameter	2.22 \pm 0.055 μm	1.36 \pm 0.052 μm
Mechanical strength:		
Young's modulus (Y)	86.56 \pm 10.33 MPa	46.70 \pm 4.66 MPa
Tensile strength	3.15 \pm 0.592 MPa	2.43 \pm 0.591 MPa
Elongation (%)	44.28 \pm 3.31	43.01 \pm 2.92
Thermal stability:		
Melting temperature (T_m)	175.18 $^{\circ}\text{C}$	178.958 $^{\circ}\text{C}$
Resistivity ρ ($\Omega\text{-cm}$):		
Dehydrated/Dry	0.78 $\times 10^8 \Omega\text{-cm}$	411.61 $\Omega\text{-cm}$
Conductivity σ (S/cm):		
Dehydrated/dry	12.8079 $\times 10^{-9}$ S/cm	2.42 $\times 10^{-3}$

	**Insulator	**Semiconductor
Mathematically derived from the slope of V/I curve		
Resistivity ρ (Ω -cm):	n/a	1.1785 Ω -cm
Conductivity σ (S/cm):	n/a	848.5123x10 ⁻³ S/cm
Wettability measurement:		
Contact angle (in degrees)	100.03 \pm 1.24°	61.82 \pm 3.40°

Table 1: Physicochemical measurements of PHB and melanin-PHB nanofiber scaffolds.

3.2. Chemical analysis and tracing of fibers elemental composition

We looked at FTIR transmittance spectra of PHB and melanin-PHB fibers to identify the characteristic peaks of functional groups, which would confirm the presence of PHB and melanin in our fibers. An initial chemical analysis of PHB and melanin in polymeric powder form suggested the presence of a characteristic aliphatic -OH stretching peak at 3436.88 cm⁻¹ and an aromatic -OH stretching peak at 3377.09 cm⁻¹ in PHB and melanin respectively (**Figure S2A and S2B**) [55]. The amine group identified in blended fibers suggests the presence of melanin and justifies their solubility in polar solvents. Indeed, water solubility of amines is largely due to their capability for hydrogen bonding [56]. Further, we observed a sp³-CH stretching peak of CH₂ and CH₃ groups in PHB at 2977.86 cm⁻¹ (**Figure S2A**) [57] and an aromatic -NH stretch of secondary amine peak in melanin at 3213.16 cm⁻¹ (**Figure S2B**) [58]. A carboxylic -C=O stretching peak was observed in PHB and melanin at 1726.15 cm⁻¹ and 1716.51 cm⁻¹ respectively [59]. We then confirmed the presence of similar peaks in PHB and melanin-PHB electrospun fibrous scaffolds. Indeed, PHB fibers were characterized by an aliphatic -

OH stretching peak at 3436.5 cm^{-1} , a sp^3 -CH stretching peak of CH_2 and CH_3 at 2975.6 cm^{-1} and carboxylic acid -C=O stretching peak at 1720.17 cm^{-1} (**Figure 2A**), with a shift of $\sim 0.38\text{ cm}^{-1}$, $\sim 2.26\text{ cm}^{-1}$ and $\sim 5.98\text{ cm}^{-1}$ compared to PHB powder (**Figure 2A and Figure S2A**). A broad primary amine peak at 3207.01 cm^{-1} , a sp^3 -CH stretching peak at 2975.06 cm^{-1} and a carboxylic acid -C=O stretching peak at 1722.10 cm^{-1} were observed in melanin-PHB fibers (**Figure 2B**), with a significant shift in peak value of $\sim 6.06\text{ cm}^{-1}$ and $\sim 5.59\text{ cm}^{-1}$ in the primary amine peak and -C=O stretching peak, compared to melanin powder (**Figure S2B**) [60]. We hypothesize that such shifts could be the result of the use of HFIP and DMSO (3:1) as solvent for the melanin-solution (4% w/v) and successful blending with PHB polymeric solution (9% w/v). We didn't observe the characteristic -NCO peak (2264 cm^{-1}) of HFIP in the fibers, suggesting successful evaporation of solvent [61], [62].

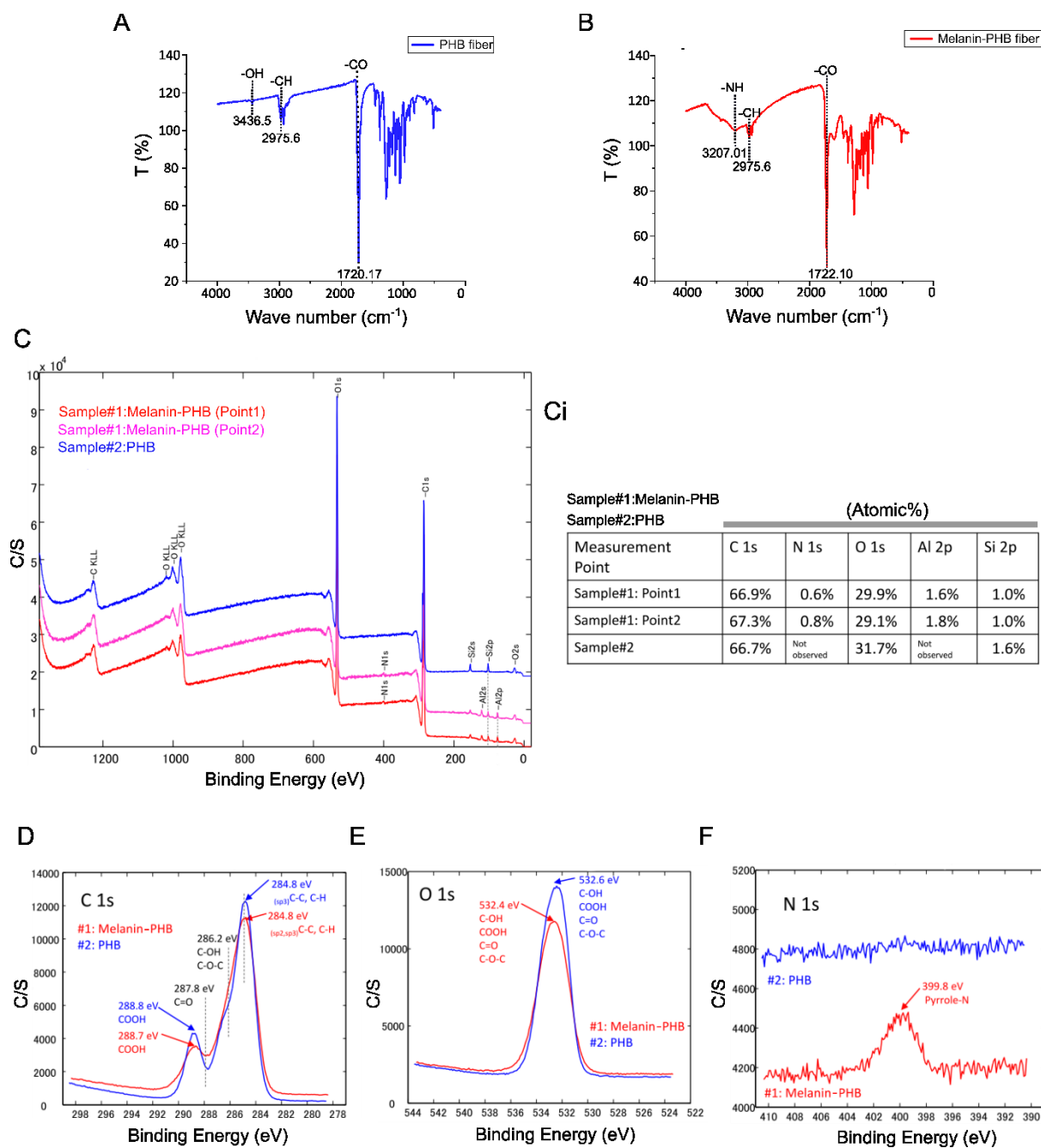


Figure 2: Chemical characterization of PHB and melanin-PHB fibers. FTIR spectra of (A) PHB fibers, and (B) melanin-PHB fibers showing the characteristic peaks of the identified functional groups. (C) XPS spectra for the elemental analysis, and (Ci) (%) atomic constitution of melanin-PHB and PHB fibers. XPS spectra shows the peak for elements (D) C1s, (E) O1s and (F) N1s in the PHB and melanin-PHB scaffolds.

This article is protected by copyright. All rights reserved.

Elemental composition analysis via X-ray photoelectron spectroscopy (XPS) of PHB and melanin-PHB was performed (**Figure 2C-2F**), highlighting the presence of similar levels of C1s (**Figure 2D**) and O1s (**Figure 2E**) in both, and confirming the presence of the common polymeric group of PHB. Further, C1s peak of sp^3 -C-C and -C-H stretching peak were located at ~ 284.8 eV (**Figure 2D**). We observed the presence of a carbonyl -C=O stretching peak between ~ 286 - 287 eV. Similarly, we detected a carboxylic acid -C=O stretching peak at 288.8 eV in both PHB and melanin-PHB fibers (**Figure 2D**). An O1s peak of carboxylic acid -C=O was also observed at ~ 532.6 eV (**Figure 2E**). The N1s peak of primary and secondary amines located at ~ 399.8 eV (**Figure 2F**) was present only in melanin blended fibers, confirming the successful blending of melanin in melanin-PHB fibers.

We also traced fiber composition by SEM-EDX analysis [34], [35] (**Figure S2 C-F**). We focused on the localization of nitrogen to map the distribution of melanin in blended fibers, since it is present in melanin and absent in PHB. We compared fibers obtained by electrospinning of 9% PHB (control sample) and a 13% blend of PHB and melanin (9% PHB and 4% melanin) (**Figure S2 C-D**) [35]. Indeed, the characteristic peak of carbon ($K\alpha$ 277 eV) and oxygen ($K\alpha$ 525 eV) was detected in both samples, while nitrogen ($K\alpha$ 392 eV) was present only in melanin-PHB fibers (**Figure S2 E-F**).

3.3. Mechanical properties

The mechanical properties of PHB and melanin-PHB fibers were investigated to verify whether these scaffolds have the required rigidity to sustain their morphology in an *in-vivo* setting. We performed atomic force microscopy (AFM) scans to determine the fiber's topology (**Figure 3A**) and DMT modulus/ Young's modulus (Y) (**Figure 3B**) to visualize the topographic distribution of mechanical strength throughout the scaffolding surface. The average topographic distribution of Young's modulus for PHB and melanin-PHB nanofibers was around ~ 70 MPa and ~ 50 MPa respectively (**Figure 3B**) [4]. We also investigated the dehydrated form of both fibrous scaffolds using a mechanical testing machine (**Table 1; Figure S1**). In that context, PHB fibers were shown to have the higher values of modulus, 46.70 ± 4.66 MPa, compared to melanin-PHB fibers, 86.56 ± 10.33 MPa (**Figure S1C**) [15], [16]. Though blending of melanin with PHB seemed to decrease the tensile

strength compared to PHB fibers (2.43 ± 0.591 MPa and 3.15 ± 0.592 MPa respectively), the difference observed was not statistically significant (**Figure S1D**). The elongation (%) showed similar values for melanin-PHB (43.01 ± 2.92 %) compared to PHB nanofibers (44.28 ± 3.31 %) (**Figure S1E**). Our data confirmed that the mechanical strength of both PHB and melanin-PHB fibers meets the physiochemical requirements for medical implants in brain-like tissues, suggesting that they would be able to sustain their spatial architecture *in-vivo* and are, thus, suitable as implants for neural soft tissues engineering [1], [25].

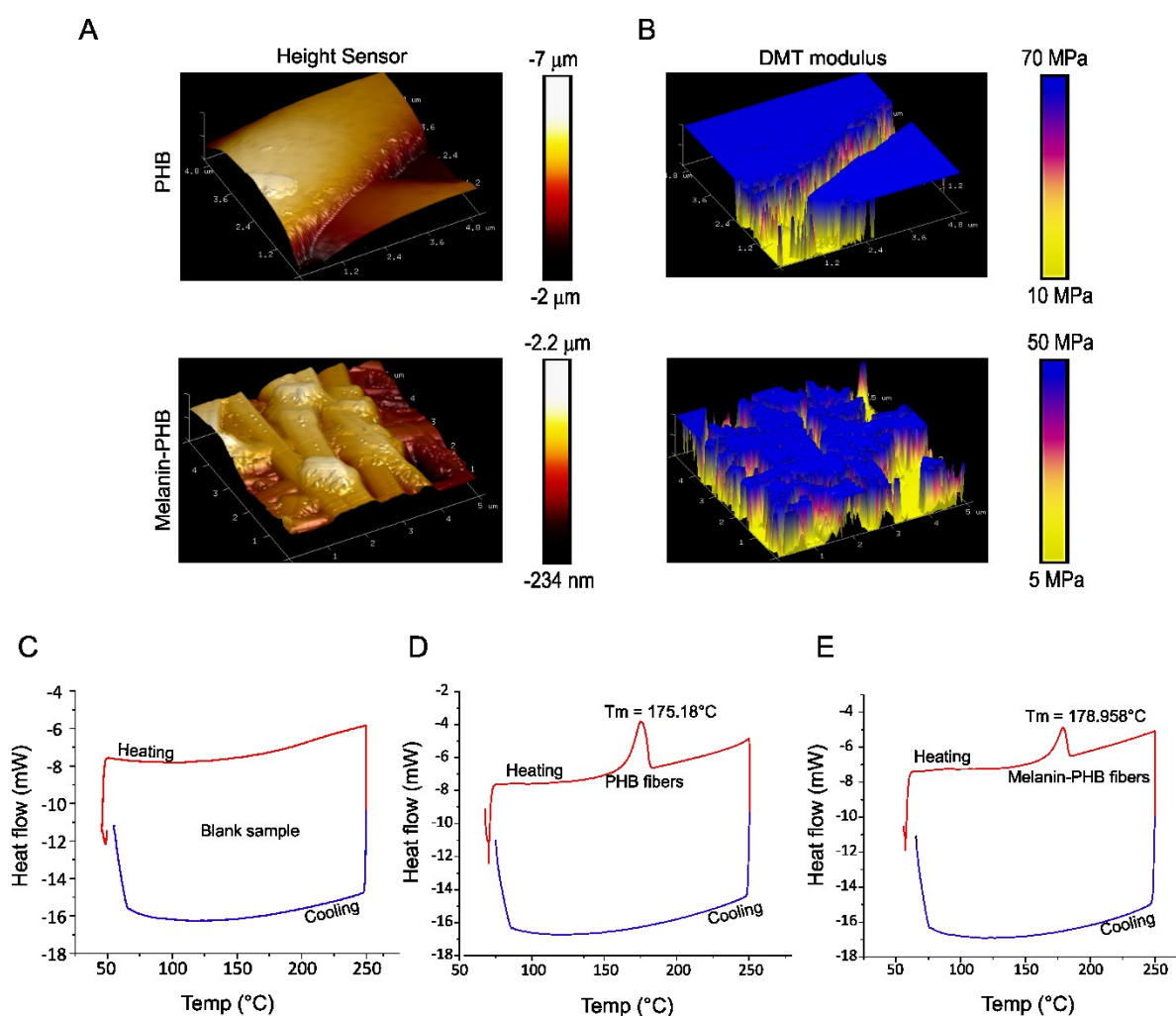


Figure 3: Mechanical and thermal property analysis of PHB and melanin-PHB fibers. (A) Representative height sensor AFM images of PHB fibers and melanin-PHB blended fibers show the surface morphology of the fibers. (B) Nanoindentation images with peak-force mode show the

topographic distribution of the calculated Young's modulus (DMT modulus). Differential scanning calorimetry (DSC) curves of a (C) blank sample, (D) PHB scaffold and (E) melanin and PHB blended fibers Heating cycle is represented in red and cooling cycle in blue color. T_m shows the peak of melting temperature.

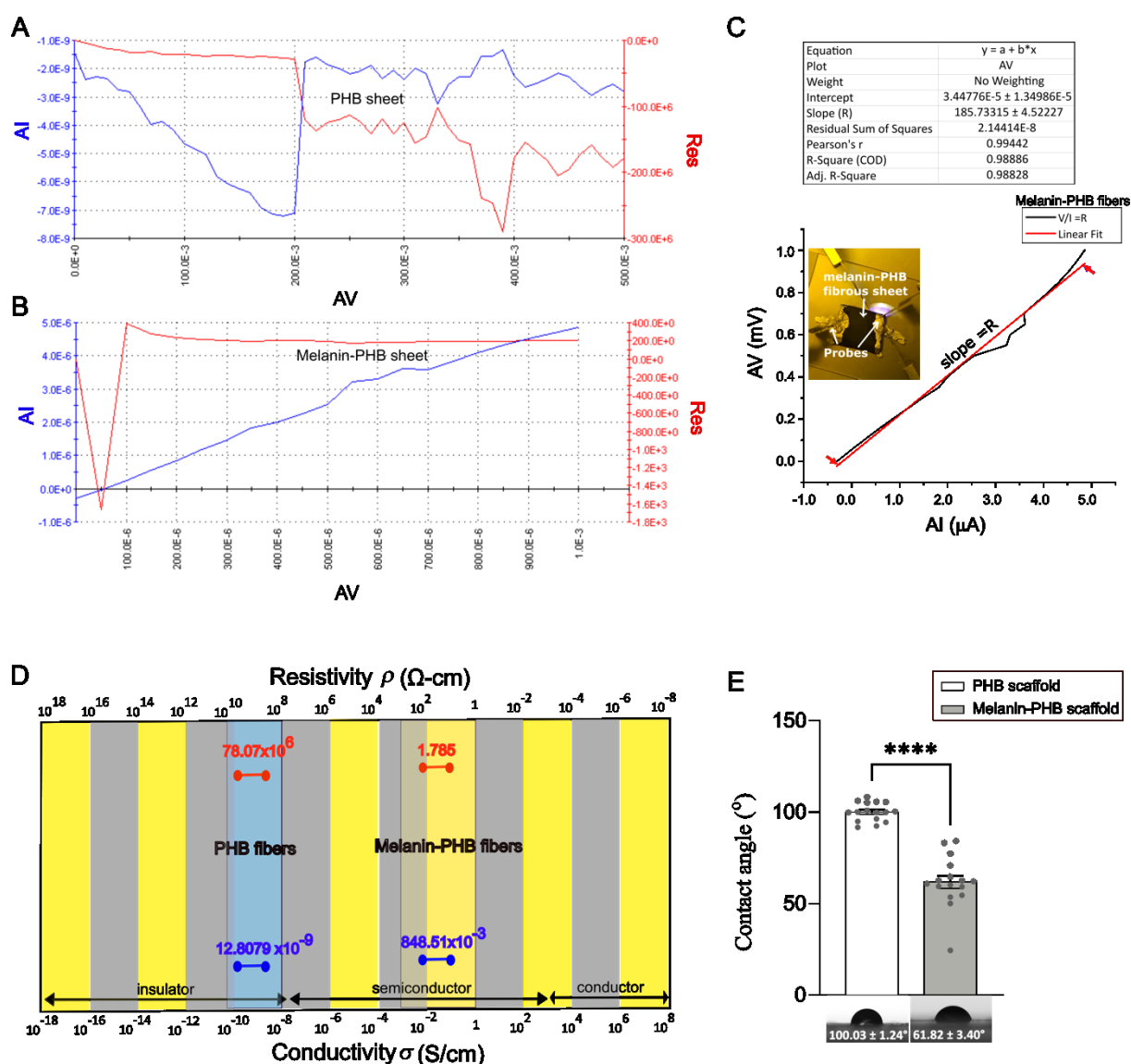
3.4 Thermal properties

Biomaterials thermal properties, such as low impedance for neural probes and durability for scaffolds, are crucial to their suitability for neural tissues applications [1], [63]. To determine the thermal properties of PHB and melanin-PHB scaffolds, we performed a calorimetry study with a differential scanning calorimeter (material and methods section 2.4.4). We observed a negative peak during the heating cycle, corresponding to the melting temperature (T_m) of the nanofibers, suggesting a deformation in the fiber structure, whereas no peak was observed during the cooling cycle, indicating that the polymer does not further undergo a state change after melting (Figure 3C-3E). The calculated T_m of PHB fibers and melanin-PHB fibers were 175.18°C (Figure 3D) and 178.95°C (Figure 3E) respectively. Elevation in T_m for melanin-PHB fibers confirmed successful blending. Our analysis suggests that melanin-PHB fibers are thermally stable and thus a suitable candidate for neural tissue engineering.

3.5 Resistivity and conductivity measurement

We explored the electrical properties of PHB and melanin-PHB fibers by measuring their resistivity (ρ) and conductivity (σ) (Figure 4A-4D). Resistivities were directly measured by 2-probes (material and method section 2.4.5). PHB and melanin-PHB fibers resistivities were $0.78 \times 10^8 \Omega\text{-cm}$ and $411.61 \Omega\text{-cm}$ respectively, while conductivities were $12.80 \times 10^{-9} \text{ S/cm}$ and $2.42 \times 10^{-3} \text{ S/cm}$ respectively (Table 1). The conductivity value for PHB fibers lies in the range of insulator materials, whereas melanin-PHB sheets were within the range of semiconductor materials (Figure 4D). Further, we confirmed the conductivity values by mathematically deriving the resistivity/conductivity values from the sheet resistance, which was calculated from the slope of the linear segment of the V/I curve as explained in the material and method section 2.4.5. We could observe a linear behavior of the V/I curve only

for melanin-PHB fibrous scaffolds (PHB alone is not conducting). Therefore, following the **equation (3)** of method **section 2.4.5**, we could derive the value of the sheet resistance ($R_s = 4.53236 \times \text{slope} = 841.80 \Omega$) from the slope (185.73315Ω) of the V/I curve for melanin-PHB sheets only. Further, we calculated the resistivity ($\rho = 1.1785$) of melanin-PHB fibrous sheets as a product of the sheet's resistance (R_s) and thickness ($t_f = 14 \mu\text{m}$). Finally, conductivity (848.51×10^{-3}) was measured as the inverse of resistivity. The calculated resistivity and conductivity of melanin-PHB sheets lies in the range of semiconductor materials (**Figure 4D**).



This article is protected by copyright. All rights reserved.

Figure 4: Electrical properties of PHB and melanin-PHB fibers using 2-probes methods. Resistivity measurement of (A) PHB and (B) melanin-PHB fibers using V vs I curve. PHB fibers behaves like as an insulator and melanin-PHB scaffolds show semiconductor like behavior. (C) Melanin-PHB sheet resistance (R_s) calculation by slope measurement of V/I curve. (D) Graphical representation of the calculated resistivity and conductivity of PHB and melanin-PHB scaffolds on the conductivity scale. (E) Contact angle measurement for the wettability/hydrophilicity analysis of PHB scaffold and melanin-PHB scaffolds. Data are shown as mean \pm s.e.m.; asterisks indicate statistical significance (Student t-test; **** $p \leq 0.0001$).

3.6 Wettability

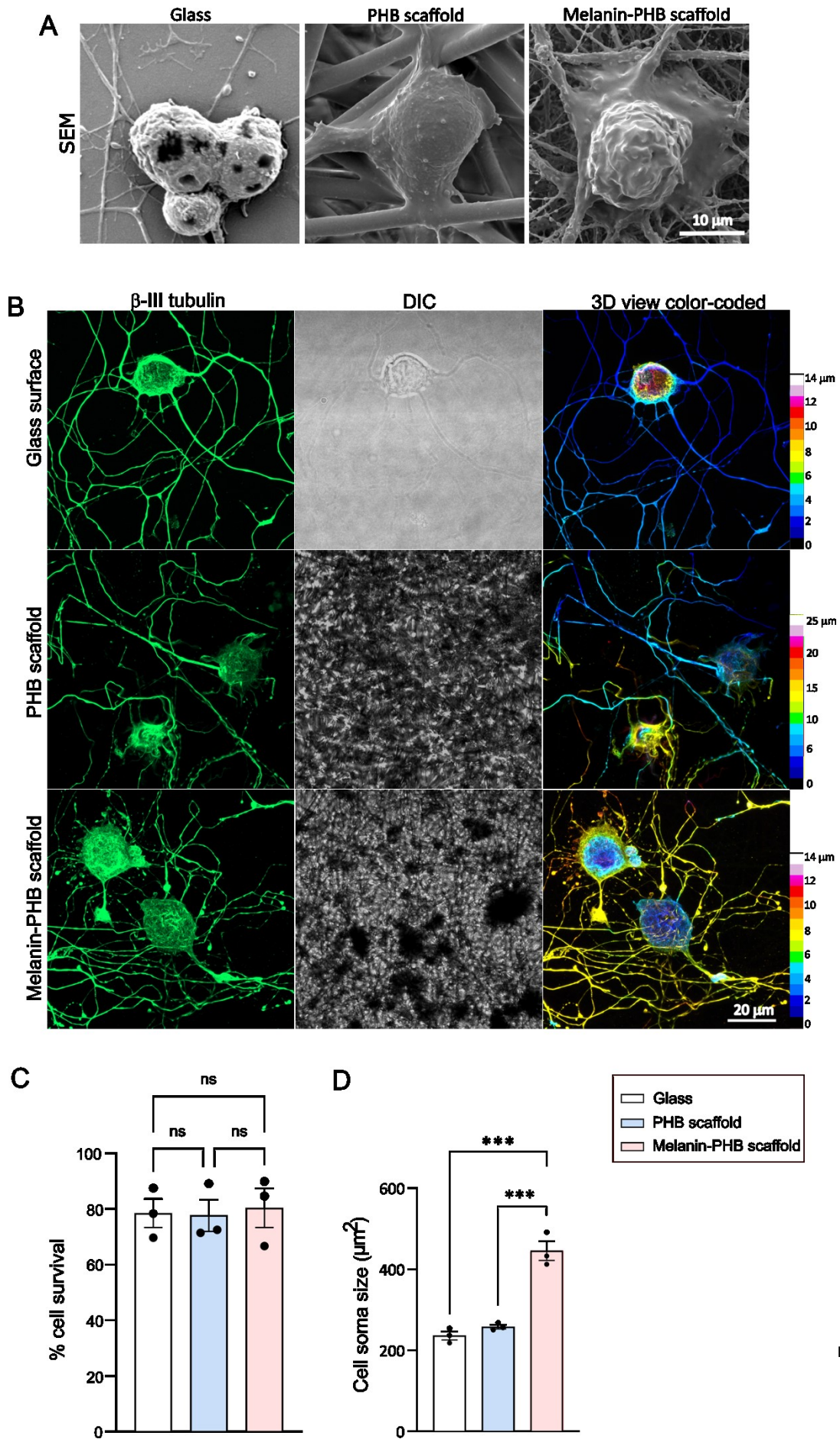
We determined the wettability (or hydrophilicity) of PHB and melanin-PHB scaffolds. The water contact angle is an important parameter to predict the adhesion of cells to the scaffold and is critical to define the its suitability for biological applications [4], [63], [64]. Surfaces displaying contact angles lower than 90° are considered hydrophilic. Our findings showed that the value of the contact angles for pure PHB fibers was significantly higher ($100.03 \pm 1.24^\circ$, ** $p < 0.0001$) than the one of melanin-PHB scaffolds ($61.82 \pm 3.40^\circ$) (**Figure 4E**), suggesting that blending of melanin increased the hydrophilicity of the resulting fibers, possibly improving protein adsorption and cell adhesion on the scaffolding surface [65], [66].

3.7 Swelling and degradation analysis

We measured the degree of swelling or swelling capacity (%) of PHB and melanin-PHB scaffolds over a period of 24h (**Figure S3 A-E**). We found the (%) swelling capacity of melanin-PHB fibers (800.58 ± 41.7) to be significantly higher (** $p \leq 0.01$) than the one of PHB fibers (169.33 ± 11.74) after 24h incubation in phosphate-buffered saline (PBS) (**Figure S3C**). We also analyzed the degradation of PHB (**Figure S3F**) and melanin-PHB fibers (**Figure S3G**) by measuring weight loss after immersion in PBS for 120 days (**Fig. S3 F-J**). Blending of melanin increased the percentage of degradation of melanin-PHB scaffolds (** $p \leq 0.01$) compared to PHB ones (**Figure S3H**).

3.8 Biocompatibility of PHB and melanin-PHB scaffolds

Dorsal root ganglia (DRG) and motor neurons (MNs) are typically affected in traumatic peripheral nerve injuries and spinal cord injuries [67], [68] [69]. We tested the biocompatibility of PHB and melanin-PHB fibrous scaffolds on both neuronal cell types *in-vitro*. SEM and fluorescence images confirmed that both DRGs (**Figure 5** and **Figure S4**) and MNs (**Figure S5**) could grow and survive on PHB or melanin-PHB scaffolds. Further, 3D representation of DRG neuronal culture on PHB and melanin-PHB scaffolds showed how axons could extend between different layers of the 3D scaffolds (**Figure 5B**). Due to their smaller soma size, MNs could pass through different layers in the 3D scaffold and extend neurite network in 3D (**Figure S5**), as shown in SEM micrographs (**Figure S5A**) and by immunofluorescence analysis (**Figure S5B**).



oved.

Figure 5: Biocompatibility of PHB and melanin-PHB fiber scaffolds. (A) High resolution SEM images of DRG neurons on glass, PHB and melanin-PHB surfaces. scale bar: 10 μm . (B) Confocal images of DRG neurons growing on glass surface, and polymeric 3D fibrous sheet of PHB and melanin-PHB fibers. Cells are stained with anti- β -III tubulin antibody (green; left panel). Transmission images (middle panel) and a color-coded representation (right panel) of the neurite outgrowth in the depth of 3D scaffold are also shown. Scale bar: 20 μm , color-coded scale bar showing the correspondence between the depth in the scaffolds and the color in the 3D view color-coded panel (C). Cell survival assay shows no significant difference in the (%) survival of DRG neurons on control glass surface, and polymeric 3D fibrous sheet of PHB and melanin-PHB. (D) Quantification of the spread of the soma on control glass surface, and polymeric 3D fibrous sheet of PHB and melanin-PHB (C-D). Data are shown as mean \pm s.e.m.; asterisks indicate statistical significance (One-way ANOVA with Tukey's post hoc test; *** $p \leq 0.001$; ns= not significant).

We also quantified the survival of DRG neurons on these substrates using a cell survival assay (**Figure S4**). No noticeable effects on neuronal viability or sign of axonal stress were observed when comparing PHB and melanin-PHB nanofibers to a silica substrate, which is standard for the culture of these neuronal types (**Figure 5C**). High resolution SEM micrographs highlighted a better attachment of DRG neurons to melanin-PHB fibers, which can be inferred by the significant increase of DRG neurons somatic area ($445.32 \pm 19.4 \mu\text{m}^2$, *** $p < 0.001$), in melanin-PHB scaffolds relative to glass ($236.25 \pm 8.48 \mu\text{m}^2$) and PHB sheets ($257.89 \pm 4.13 \mu\text{m}^2$) (**Figure 5A and 5D**). Thus, our data support the biocompatibility of melanin blended PHB scaffolds and their suitability for neuronal cultures.

Discussion

Several millions of people worldwide are affected by peripheral nerve injury (PNI), spinal cord injury (SCI), and traumatic brain injury (TBI) [70], [71]. Autologous nerve grafts have been used to address these clinical needs, but their successful implementation has been hampered by limitations such as

donor site morbidity, potential loss of function, and limited amount of tissue graft [8], [71]. Thus, alternative strategies are actively being investigated. Over the past decades, tissue engineering has gained attention as an alternative to conventional transplant methods [8]. The viscoelastic and conducting nature of nerve cells makes the development of a suitable polymer formulation for scaffolds challenging [1]. Though several classes of biomaterials have been investigated to improve regeneration of damaged neural tissue, electrical cues and biodegradability have been difficult to achieve and need to be addressed in order to enable the development of effective scaffolds [1], [23], [25], [72], [73]. To date, most of NTE applications are in pre-clinical phase, with the exception of collagen-based conduits, which have been successfully tested in clinical trials for regeneration of peripheral nerves [74], [75]. Most biomaterials available are not electrically conductive, a property crucial for neural tissues [76], [77], [7], [10]. Indeed, direct electrophysiological link between nerve cells and electrical stimulation was shown to influence cell signaling and protein adsorption [15], though, the exact mechanism is not yet clear [7]. Numerous, electrically conductive polymers have been investigated, including polypyrrole (PPy), polyaniline (PANI), poly(3,4- ethylenedioxythiophene), polystyrene sulfonate (PEDOT: PSS), poly(3-hexylthiophene) (P3HT), poly(2,2'-bithiophene) (PBP), and polythiophene and poly(para-phenylenevinylene), which are biocompatible but non-biodegradable [76], [72], [2], [3], [78].

In our previous works, we investigated the effect of varying the degree of alignment of electrospun fibrous scaffolds on neuronal cell behavior [19], and controlled geometry on directional axonal growth, using IP-DIP photo-resin lithographed 3D-scaffolds [4]. In the present study, we developed electrospun electrically conductive and biodegradable fibrous scaffolds by blending the natural pigment melanin with the natural polymer poly-3-hydroxybutyrate (PHB). PHB is biodegradable and has been used in healthcare such as surgical sutures, nerve repair, and drug delivery [79], [80], [77], [81], [31]. Melanins are naturally occurring conductive pigments, chemically characterized as heteropolymers of 5,6-dihydroxyindole and 5,6-dihydroxyindole-2-carboxylic acid. The electrical conductivity of melanin ranges from $10^{-8} \text{ S cm}^{-1}$ in the dehydrated state up to 10^{-3} Scm^{-1} in the fully hydrated state [82], [15], [83]. Herein, the unique properties of melanin and PHB polymers were explored to construct conducting and biodegradable nanofiber scaffolds with potential for NTE applications. Physicochemical analysis confirmed successful fabrication of melanin blended PHB fibers using electrospinning (**Figure 1**). Electrospun melanin-PHB scaffolds were shown

to provide a larger surface area and better cell attachment due to their rough surface and the presence of nanometer size fibers in the mesh [4], [76], [84] (**Figure 1**). The ideal mechanical strength of brain tissue ranges from few hundreds of Pa to MPa [1]. It has been reported that mechanical mismatch between engineered biomaterial and brain tissue can cause mechano-chemical inflammation and injuries through the activation of apoptotic cellular pathways [1], [85]. Therefore, materials developed for NTE should also have neuroprotective properties [23], [26]–[28]. Our material is composed of melanin, which is a well-known neuroprotective substance [26], [28]. The stiffness of our engineered biomaterial measured in terms of elastic moduli, tensile strength and elongation (%) lies in the ideal range for brain tissues engineering (**Figure 3B** and **Figure S1**) [1], [9], [23]. In addition, calorimetry investigation with DSC showed that our biomaterial is thermally stable and can sustain high temperatures (**Figure 3E**). Adding melanin has not only increased the hydrophilicity (**Figure 4E**), swelling and biodegradability (**Figure S3**) of nanofibers due to the presence of polar functional groups (**Figure 2B**), but also made the fibers conducting in nature, opening to the possible use of melanin for bioelectronics (**Figure 4B-4D; Table 1**) [86]. Conductive scaffolds will facilitate the establishments of electrical cues in an *in-vivo* setting, which might accelerate neuronal growth [7]. Melanin-PHB fibers are also mechanically and thermally stable (**Figure 3**) and might reduce impedance due to a larger surface area for ionic-electronic transduction. These properties might make the melanin-PHB blend suitable for the coating of neural probes and semiconducting circuitry on chips for brain machine interfacing [1], [15], [23], [82]. Further, melanin-PHB fibers rough surface and conductive nature facilitated the attachment [4] and survival of mouse sensory (**Figure 5**) and motor neurons (**Figure S5**), without impacting cell viability (**Figure 5C** and **Figure S4**). High resolution SEM micrographs showed a better attachment of DRG neurons on melanin-PHB fibers, as evidenced by the flattening of the neuronal soma and the significant increase in the cell body area (**Figure 5A** and **5D**). The observed improvement in cell adhesion might be the product of melanin-PHB scaffolds topological features, such as surface roughness, micropores [87], [88] surface energy of substrate [89], [90], and increased swelling capacity/hydrophilicity [91], [92], in conjunction with laminin coating, which might have promoted the interaction between scaffold and cell surface receptor proteins, like integrin, known to facilitate neuronal growth [11], [93]–[95]. Indeed, surface modifications that increase the nanoscale roughness of electrospun fibers have been reported to improve cell attachment, differentiation and proliferation regardless of cell type [84], [89], [96]. A recent study also showed how melanin-based electroactive and antioxidant silk-fibroin nanofibrous

scaffolds displayed neuroprotective properties, and improved cell proliferation and differentiation of neuroblastoma cells [23]. Taken together, our data suggests the suitability and potential advantages of melanin-PHB scaffold as a brain-tissue-like biomaterial, which could be deployed to repair damaged neural tissue and support the regrowth of severed nerves.

Conclusions

In this study, we successfully fabricated biodegradable and conductive fibrous scaffolds, using a blend of melanin and PHB. These fibers were characterized for their physical and chemical properties. Melanin blending favorably altered PHB fibers morphology, diameter and wettability and positively improved their electrical conductivity. These scaffolds were also shown to be thermally stable, while providing suitable tensile properties, porous network, high surface area to volume ratio, and being able to support the growth of DRG and motor neurons. Indeed, melanin-PHB fibers were biocompatible and did not impact neuronal survival, while improving cell adhesion, as shown by the observed increase in somatic area. The measured physiochemical and electrical properties, coupled with the observed biocompatibility and biodegradability, suggest that our melanin-PHB scaffolds could be applied to neural tissue engineering applications. Future pre-clinical *in-vivo* studies are required to predict the feasibility of clinical use.

Acknowledgements

We acknowledge Nagano Shoko and Ohata Hirohito for their technical help in data collection with SHIM and XPS at the open facility platform National Institute of Material Sciences (Japan), and OIST engineering support section staff Hyung Been Kang, Takuya Miyazawa, Menouer Saidani and Toshiaki Mochizuki for their technical help during the data collection with FTIR, Bruker AFM, Keithley 2-probe and elemental tracing with SEM-EDX. We also acknowledge the help from Laurent Guillaud in imaging with the confocal microscope and edits in the manuscript, and Miki Otsuki for the preparation of DRG cultures.

Contributions

MT, SKV, and LA conceived the project, performed the experiments, collected the data, and drafted the manuscript. TS helped in the development of idea and participated in the editing of manuscript. PB performed part of the imaging and participated in the editing of the manuscript.

Data availability statement

We have provided the data required for the publication. The raw/processed data required to reproduce these findings cannot be shared at this time as the data also forms part of an ongoing study but will be shared upon publication.

Funding

TS acknowledges the support of Grant-in-Aid for Scientific Research (#26640024) from the Ministry of Education, Culture, Sports, Science, and Technology (MEXT) of Japan. MT acknowledges the support by KICKS2020 internal funding initiative from the Okinawa Institute of Science and Technology Graduate University and JSPS/Kakenhi C Research Grant (#20K07458) in the current study.

Declaration of conflict of interest

The authors declared no potential conflicts of interest with respect to the research, authorship, and/or publication of this article.

Informed Consent

This article is protected by copyright. All rights reserved.

All authors have read the final draft and approved the submission to the journal.

Ethics approval statement:

All experiments were performed following the guidelines of the Okinawa Institute of Science and Technology Graduate University (OIST) genetic manipulation procedures. All animal experiments were performed in accordance with the regulations of OIST animal care and use committee (protocol #2021-326). OIST animal facilities and animal care and use program are accredited by AAALAC International (Ref. #1551).

Patient consent statement: N/A

Permission to reproduce material from other sources: N/A

Clinical trial registration: N/A

References

- [1] E. Axpe, G. Orive, K. Franze, and E. A. Appel, "Towards brain-tissue-like biomaterials," *Nat. Commun.*, vol. 11, no. 1, p. 3423, Jul. 2020, doi: 10.1038/s41467-020-17245-x.
- [2] L. R. Doblado, C. Martínez-Ramos, and M. M. Pradas, "Biomaterials for Neural Tissue Engineering," *Front. Nanotechnol.*, vol. 3, 2021, [Online]. Available: <https://www.frontiersin.org/article/10.3389/fnano.2021.643507>
- [3] F. Pires, Q. Ferreira, C. A. V. Rodrigues, J. Morgado, and F. C. Ferreira, "Neural stem cell differentiation by electrical stimulation using a cross-linked PEDOT substrate: Expanding the use of biocompatible conjugated conductive polymers for neural tissue engineering," *Biochim. Biophys. Acta BBA - Gen. Subj.*, vol. 1850, no. 6, pp. 1158–1168, Jun. 2015, doi: 10.1016/j.bbagen.2015.01.020.

This article is protected by copyright. All rights reserved.

- [4] L. Agrawal, M. Saidani, L. Guillaud, and M. Terenzio, "Development of 3D culture scaffolds for directional neuronal growth using 2-photon lithography," *Mater. Sci. Eng. C*, vol. 131, p. 112502, Dec. 2021, doi: 10.1016/j.msec.2021.112502.
- [5] R. Ng, R. Zang, K. K. Yang, N. Liu, and S.-T. Yang, "Three-dimensional fibrous scaffolds with microstructures and nanotextures for tissue engineering," *RSC Adv.*, vol. 2, no. 27, pp. 10110–10124, 2012, doi: 10.1039/C2RA21085A.
- [6] Z. Tong, M. Segura-Feliu, O. Seira, A. Homs-Corbera, J. A. Del Río, and J. Samitier, "A microfluidic neuronal platform for neuron axotomy and controlled regenerative studies," *RSC Adv.*, vol. 5, no. 90, pp. 73457–73466, 2015, doi: 10.1039/C5RA11522A.
- [7] P. Sikorski, "Electroconductive scaffolds for tissue engineering applications," *Biomater. Sci.*, vol. 8, no. 20, pp. 5583–5588, 2020, doi: 10.1039/D0BM01176B.
- [8] Y. Gao *et al.*, "Nerve autografts and tissue-engineered materials for the repair of peripheral nerve injuries: a 5-year bibliometric analysis," *Neural Regen. Res.*, vol. 10, no. 6, pp. 1003–1008, Jun. 2015, doi: 10.4103/1673-5374.158369.
- [9] R. C. Young, G. Terenghi, and M. Wiberg, "Poly-3-hydroxybutyrate (PHB): a resorbable conduit for long-gap repair in peripheral nerves," *Br. J. Plast. Surg.*, vol. 55, no. 3, pp. 235–240, Apr. 2002, doi: 10.1054/bjps.2002.3798.
- [10] H. Nekounam *et al.*, "Electroconductive scaffolds for tissue regeneration: Current opportunities, pitfalls, and potential solutions," *Mater. Res. Bull.*, vol. 134, p. 111083, Feb. 2021, doi: 10.1016/j.materresbull.2020.111083.
- [11] C. S. Barros, S. J. Franco, and U. Müller, "Extracellular matrix: functions in the nervous system," *Cold Spring Harb. Perspect. Biol.*, vol. 3, no. 1, pp. a005108–a005108, Jan. 2011, doi: 10.1101/cshperspect.a005108.
- [12] V. P. Baklaushev *et al.*, "Tissue Engineered Neural Constructs Composed of Neural Precursor Cells, Recombinant Spidroin and PRP for Neural Tissue Regeneration," *Sci. Rep.*, vol. 9, no. 1, p. 3161, Feb. 2019, doi: 10.1038/s41598-019-39341-9.
- [13] A. Wolfberger *et al.*, "Photolithographic patterning of cellulose: a versatile dual-tone photoresist for advanced applications," *Cellulose*, vol. 22, no. 1, pp. 717–727, Feb. 2015, doi: 10.1007/s10570-014-0471-4.
- [14] Y. Chen, K. Lee, N. Kawazoe, Y. Yang, and G. Chen, "ECM scaffolds mimicking extracellular matrices of endochondral ossification for the regulation of mesenchymal stem cell differentiation," *Acta Biomater.*, vol. 114, pp. 158–169, Sep. 2020, doi: 10.1016/j.actbio.2020.07.049.

- [15] C. J. Bettinger, J. P. Bruggeman, A. Misra, J. T. Borenstein, and R. Langer, “Biocompatibility of biodegradable semiconducting melanin films for nerve tissue engineering,” *Biomaterials*, vol. 30, no. 17, pp. 3050–3057, Jun. 2009, doi: 10.1016/j.biomaterials.2009.02.018.
- [16] G. Shi, Z. Zhang, and M. Rouabhia, “The regulation of cell functions electrically using biodegradable polypyrrole-poly lactide conductors,” *Biomaterials*, vol. 29, no. 28, pp. 3792–3798, Oct. 2008, doi: 10.1016/j.biomaterials.2008.06.010.
- [17] M. P. Prabhakaran, L. Ghasemi-Mobarakeh, G. Jin, and S. Ramakrishna, “Electrospun conducting polymer nanofibers and electrical stimulation of nerve stem cells,” *J. Biosci. Bioeng.*, vol. 112, no. 5, pp. 501–507, Nov. 2011, doi: 10.1016/j.jbiosc.2011.07.010.
- [18] N. Srivastava, J. James, and K. S. Narayan, “Morphology and electrostatics play active role in neuronal differentiation processes on flexible conducting substrates,” *organogenesis*, vol. 10, no. 1, pp. 1–5, 2014.
- [19] S. K. Vimal, N. Ahamad, and D. S. Katti, “A simple method for fabrication of electrospun fibers with controlled degree of alignment having potential for nerve regeneration applications,” *Mater. Sci. Eng. C*, vol. 63, pp. 616–627, Jun. 2016, doi: 10.1016/j.msec.2016.03.008.
- [20] A. Mobasser, A. Faroni, B. M. Minogue, S. Downes, G. Terenghi, and A. J. Reid, “Polymer Scaffolds with Preferential Parallel Grooves Enhance Nerve Regeneration,” *Tissue Eng. Part A*, vol. 21, no. 5–6, pp. 1152–1162, Mar. 2015, doi: 10.1089/ten.tea.2014.0266.
- [21] M. Keshavarz *et al.*, “Induced neural stem cell differentiation on a drawn fiber scaffold—toward peripheral nerve regeneration,” *Biomed. Mater.*, vol. 15, no. 5, p. 055011, Jul. 2020, doi: 10.1088/1748-605x/ab8d12.
- [22] B. B. Patel, F. Sharifi, D. P. Stroud, R. Montazami, N. N. Hashemi, and D. S. Sakaguchi, “3D Microfibrous Scaffolds Selectively Promotes Proliferation and Glial Differentiation of Adult Neural Stem Cells: A Platform to Tune Cellular Behavior in Neural Tissue Engineering,” *Macromol. Biosci.*, vol. 19, no. 2, p. 1800236, Feb. 2019, doi: 10.1002/mabi.201800236.
- [23] M. Nune, S. Manchineella, G. T., and N. K.S., “Melanin incorporated electroactive and antioxidant silk fibroin nanofibrous scaffolds for nerve tissue engineering,” *Mater. Sci. Eng. C*, vol. 94, pp. 17–25, Jan. 2019, doi: 10.1016/j.msec.2018.09.014.
- [24] P. Srisuk *et al.*, “Eumelanin Nanoparticle-Incorporated Polyvinyl Alcohol Nanofibrous Composite as an Electroconductive Scaffold for Skeletal Muscle Tissue Engineering,” *ACS Appl. Bio Mater.*, vol. 1, no. 6, pp. 1893–1905, Dec. 2018, doi: 10.1021/acsabm.8b00465.
- [25] L. N. Novikova, J. Pettersson, M. Brohlin, M. Wiberg, and L. N. Novikov, “Biodegradable poly-beta-hydroxybutyrate scaffold seeded with Schwann cells to promote spinal cord repair,” *Biomaterials*, vol. 29, no. 9, pp. 1198–1206, Mar. 2008, doi: 10.1016/j.biomaterials.2007.11.033.

- [26] W. Korytowski, T. Sarna, and M. Zareba, "Antioxidant Action of Neuromelanin: The Mechanism of Inhibitory Effect on Lipid Peroxidation," *Arch. Biochem. Biophys.*, vol. 319, no. 1, pp. 142–148, May 1995, doi: 10.1006/abbi.1995.1276.
- [27] N. G. Lindquist, B. S. Larsson, and A. Lydén-Sokolowski, "Neuromelanin and its possible protective and destructive properties.," *Pigment Cell Res.*, vol. 1, no. 3, pp. 133–136, 1987, doi: 10.1111/j.1600-0749.1987.tb00403.x.
- [28] A. S. ElObeid, A. Kamal-Eldin, M. A. K. Abdelhalim, and A. M. Haseeb, "Pharmacological Properties of Melanin and its Function in Health.," *Basic Clin. Pharmacol. Toxicol.*, vol. 120, no. 6, pp. 515–522, Jun. 2017, doi: 10.1111/bcpt.12748.
- [29] C. Cavallini *et al.*, "Melanin and Melanin-Like Hybrid Materials in Regenerative Medicine," *Nanomater. Basel Switz.*, vol. 10, no. 8, p. 1518, Aug. 2020, doi: 10.3390/nano10081518.
- [30] O. V. Gevorkyan, I. B. Meliksetyan, T. R. Petrosyan, and A. S. Hovsepian, "Bacterial melanin promotes recovery after sciatic nerve injury in rats," *Neural Regen. Res.*, vol. 10, no. 1, p. 124, 2015.
- [31] T. Eom, K. Woo, and B. S. Shim, "Melanin: a naturally existing multifunctional material," *Appl. Chem. Eng.*, vol. 27, no. 2, pp. 115–122, 2016.
- [32] A. Lutz, "Silk Hydrogels Incorporated with Melanin," 2021.
- [33] Y. S. L. V. Narayana, T. Yoshida, C. Chakraborty, M. K. Bera, and M. Higuchi, "Proton Conductivity of Metallo-Supramolecular Polymer Boosted by Lithium Ions," *ACS Appl. Polym. Mater.*, vol. 2, no. 2, pp. 326–334, Feb. 2020, doi: 10.1021/acsapm.9b00818.
- [34] J. J. Ahire, M. Hattingh, D. P. Neveling, and L. M. T. Dicks, "Copper-Containing Anti-Biofilm Nanofiber Scaffolds as a Wound Dressing Material," *PLOS ONE*, vol. 11, no. 3, p. e0152755, Mar. 2016, doi: 10.1371/journal.pone.0152755.
- [35] E. Pavlova, I. Nikishin, A. Bogdanova, D. Klinov, and D. Bagrov, "The miscibility and spatial distribution of the components in electrospun polymer–protein mats," *RSC Adv.*, vol. 10, no. 8, pp. 4672–4680, 2020, doi: 10.1039/C9RA10910B.
- [36] G. Lagaly, "B. V. Derjaguin, N. V. Churaev, V. M. Müller: Surface Forces, Consultants Bureau, New York, London 1987. 440 Seiten, Preis: \$ 95,00," *Berichte Bunsenges. Für Phys. Chem.*, vol. 92, no. 9, pp. 1058–1058, Sep. 1988, doi: 10.1002/bbpc.198800264.
- [37] I. T. Seoane, P. Cerrutti, A. Vazquez, V. P. Cyras, and L. B. Manfredi, "Ternary nanocomposites based on plasticized poly(3-hydroxybutyrate) and nanocellulose," *Polym. Bull.*, vol. 76, no. 2, pp. 967–988, Feb. 2019, doi: 10.1007/s00289-018-2421-z.

- [38] E. L. Sánchez-Safont, A. Aldureid, J. M. Lagarón, L. Cabedo, and J. Gámez-Pérez, “Study of the Compatibilization Effect of Different Reactive Agents in PHB/Natural Fiber-Based Composites,” *Polymers*, vol. 12, no. 9, 2020, doi: 10.3390/polym12091967.
- [39] S. Rebouillat and M. E. Lyons, “Measuring the electrical conductivity of single fibres,” *Int. J. Electrochem. Sci.*, vol. 6, no. 11, pp. 5731–5740, 2011.
- [40] M. Naftaly *et al.*, “Sheet Resistance Measurements of Conductive Thin Films: A Comparison of Techniques,” *Electronics*, vol. 10, no. 8, 2021, doi: 10.3390/electronics10080960.
- [41] P. Huo, X. Han, W. Zhang, J. Zhang, P. Kumar, and B. Liu, “Electrospun Nanofibers of Polycaprolactone/Collagen as a Sustained-Release Drug Delivery System for Artemisinin,” *Pharmaceutics*, vol. 13, no. 8, 2021, doi: 10.3390/pharmaceutics13081228.
- [42] J. Cimadoro and S. Goyanes, “Reversible swelling as a strategy in the development of smart membranes from electrospun polyvinyl alcohol nanofiber mats,” *J. Polym. Sci.*, vol. 58, no. 5, pp. 737–746, Mar. 2020, doi: 10.1002/pol.20190156.
- [43] M. Jannesari, J. Varshosaz, M. Morshed, and M. Zamani, “Composite poly (vinyl alcohol)/poly (vinyl acetate) electrospun nanofibrous mats as a novel wound dressing matrix for controlled release of drugs,” *Int. J. Nanomedicine*, vol. 6, p. 993, 2011.
- [44] M. Barbeck *et al.*, “Analysis of the in vitro degradation and the in vivo tissue response to bi-layered 3D-printed scaffolds combining PLA and biphasic PLA/bioglass components - Guidance of the inflammatory response as basis for osteochondral regeneration,” *Bioact. Mater.*, vol. 2, no. 4, pp. 208–223, Jun. 2017, doi: 10.1016/j.bioactmat.2017.06.001.
- [45] K. Ben-Yaakov *et al.*, “Axonal transcription factors signal retrogradely in lesioned peripheral nerve,” *EMBO J.*, vol. 31, no. 6, pp. 1350–1363, Mar. 2012, doi: 10.1038/emboj.2011.494.
- [46] L. Agrawal, S. K. Vimal, and T. Shiga, “Role of serotonin 4 receptor in the growth of hippocampal neurons during the embryonic development in mice,” *Neuropharmacology*, vol. 158, p. 107712, Nov. 2019, doi: 10.1016/j.neuropharm.2019.107712.
- [47] S. Dwane, E. Durack, and P. A. Kiely, “Optimising parameters for the differentiation of SH-SY5Y cells to study cell adhesion and cell migration,” *BMC Res. Notes*, vol. 6, no. 1, pp. 1–11, 2013.
- [48] N. Srivastava, V. Venugopalan, M. S. Divya, V. A. Rasheed, J. James, and K. S. Narayan, “Neuronal differentiation of embryonic stem cell derived neuronal progenitors can be regulated by stretchable conducting polymers,” *Tissue Eng. Part A*, vol. 19, no. 17–18, pp. 1984–1993, 2013.
- [49] S. H. Lim, X. Y. Liu, H. Song, K. J. Yarema, and H.-Q. Mao, “The effect of nanofiber-guided cell alignment on the preferential differentiation of neural stem cells,” *Biomaterials*, vol. 31, no. 34, pp. 9031–9039, 2010.

- [50] T. Bernas and J. Dobrucki, "Mitochondrial and nonmitochondrial reduction of MTT: Interaction of MTT with TMRE, JC-1, and NAO mitochondrial fluorescent probes," *Cytom. J. Int. Soc. Anal. Cytol.*, vol. 47, no. 4, pp. 236–242, 2002.
- [51] R. Chakrabarti, S. Kundu, S. Kumar, and R. Chakrabarti, "Vitamin A as an enzyme that catalyzes the reduction of MTT to formazan by vitamin C," *J. Cell. Biochem.*, vol. 80, no. 1, pp. 133–138, 2001.
- [52] L. Lü, L. Zhang, M. S. M. Wai, D. T. W. Yew, and J. Xu, "Exocytosis of MTT formazan could exacerbate cell injury.," *Toxicol. Vitro Int. J. Publ. Assoc. BIBRA*, vol. 26, no. 4, pp. 636–644, Jun. 2012, doi: 10.1016/j.tiv.2012.02.006.
- [53] T. L. Riss, R. A. Moravec, and A. L. Niles, "Cell viability assays In: Sittampalam GS, Coussens NP, Brimacombe K. et al., eds," *Assay Guid. Man. Bethesda MD USA Eli Lilly Co. Natl. Cent. Adv. Transl. Sci.*, 2013.
- [54] M. C. Pagliacci *et al.*, "Genistein inhibits tumour cell growth in vitro but enhances mitochondrial reduction of tetrazolium salts: a further pitfall in the use of the MTT assay for evaluating cell growth and survival," *Eur. J. Cancer*, vol. 29, no. 11, pp. 1573–1577, 1993.
- [55] C. Mitchell, G.-R. Yang, and J. Senkevich, "Adhesion aspects of poly(p -xylylene) to SiO₂ surfaces using γ -methacryloxypropyltrimethoxysilane as an adhesion promoter," *J. Adhes. Sci. Technol. - J ADHES SCI TECHNOL*, vol. 20, pp. 1637–1647, Jan. 2006, doi: 10.1163/156856106778884217.
- [56] J. Wu, Y. Huang, and X. Huang, "Efficient trap of polar aromatic amines in environmental waters by electroenhanced solid phase microextraction based on porous monolith doped with carboxylic carbon nanotubes," *Sep. Purif. Technol.*, vol. 282, p. 120067, Feb. 2022, doi: 10.1016/j.seppur.2021.120067.
- [57] N. Nagiah, L. Madhavi, R. Anitha, T. Natarajan, and U. Sivagnanam, "Electrospinning of poly(3-hydroxybutyric acid) and gelatin blended thin films: Fabrication, characterization, and application in skin regeneration," *Polym. Bull.*, vol. 70, Aug. 2013, doi: 10.1007/s00289-013-0956-6.
- [58] B. Smith, "Organic Nitrogen Compounds VIII: Imides," 2020.
- [59] S. Raveendran *et al.*, "Production and characterization of poly-3-hydroxybutyrate from crude glycerol by *Bacillus sphaericus* NII 0838 and improving its thermal properties by blending with other polymers," *Braz. Arch. Biol. Technol.*, vol. 54, pp. 783–794, Aug. 2011, doi: 10.1590/S1516-89132011000400019.
- [60] Goudappagouda, K. Asokan, R. Nayak, R. Krishnan, and S. S. Babu, "Tuning phosphorescence features of triphenylamines by varying functional groups and intermolecular interactions," *Dyes Pigments*, vol. 173, p. 107931, Feb. 2020, doi: 10.1016/j.dyepig.2019.107931.

- [61] C. Shan, C. Ning, J. Lou, W. Xu, and Y. Zhang, "Design and preparation of UV-curable waterborne polyurethane based on novel fluorinated chain extender," *Polym. Bull.*, vol. 78, Apr. 2021, doi: 10.1007/s00289-020-03202-7.
- [62] B. Czarnik-Matusiewicz, S. Pilorz, L.-P. Zhang, and Y. Wu, "Structure of hexafluoroisopropanol–water mixture studied by FTIR-ATR spectra and selected chemometric methods," *Prog. Two-Dimens. Correl. Spectrosc.*, vol. 883–884, pp. 195–202, Jul. 2008, doi: 10.1016/j.molstruc.2007.11.062.
- [63] M. Mohd Nizar, M. S. A. Hamzah, S. I. Abd Razak, and N. H. Mat Nayan, "Thermal Stability and Surface Wettability Studies of Polylactic Acid/Halloysite Nanotube Nanocomposite Scaffold for Tissue Engineering Studies," *IOP Conf. Ser. Mater. Sci. Eng.*, vol. 318, p. 012006, Mar. 2018, doi: 10.1088/1757-899x/318/1/012006.
- [64] D. J. W *et al.*, "Contact angles: history of over 200 years of open questions," *Surface Innovations*, vol. 8, no. 1–2, pp. 3–27, 2020.
- [65] S. Ito, M. Kasuya, K. Kurihara, and M. Nakagawa, "Surface forces between hydrophilic silica surfaces in a moisture-sensitive oleophilic diacrylate monomer liquid," *AIP Adv.*, vol. 8, no. 2, p. 025122, Feb. 2018, doi: 10.1063/1.4991630.
- [66] V. Tangpasuthadol, N. Pongchaisirikul, and V. P. Hoven, "Surface modification of chitosan films.: Effects of hydrophobicity on protein adsorption," *Carbohydr. Res.*, vol. 338, no. 9, pp. 937–942, Apr. 2003, doi: 10.1016/S0008-6215(03)00038-7.
- [67] H. Hou *et al.*, "Acute spinal cord injury could cause activation of autophagy in dorsal root ganglia," *Spinal Cord*, vol. 51, no. 9, pp. 679–682, Sep. 2013, doi: 10.1038/sc.2013.52.
- [68] G. Melli and A. Höke, "Dorsal Root Ganglia Sensory Neuronal Cultures: a tool for drug discovery for peripheral neuropathies," *Expert Opin. Drug Discov.*, vol. 4, no. 10, pp. 1035–1045, Oct. 2009, doi: 10.1517/17460440903266829.
- [69] A. M. G. Ragagnin, S. Shadfar, M. Vidal, M. S. Jamali, and J. D. Atkin, "Motor Neuron Susceptibility in ALS/FTD," *Front. Neurosci.*, vol. 13, 2019, [Online]. Available: <https://www.frontiersin.org/article/10.3389/fnins.2019.00532>
- [70] Y. Kang *et al.*, "Epidemiology of worldwide spinal cord injury: a literature review," *J. Neurorestoratology*, vol. Volume 6, pp. 1–9, Dec. 2017, doi: 10.2147/JN.S143236.
- [71] S. Chen *et al.*, "Repair, protection and regeneration of peripheral nerve injury," *Neural Regen. Res.*, vol. 10, no. 11, pp. 1777–1798, Dec. 2015, doi: 10.4103/1673-5374.170301.
- [72] H. Farkhondehnia, M. Amani Tehran, and F. Zamani, "Fabrication of Biocompatible PLGA/PCL/PANI Nanofibrous Scaffolds with Electrical Excitability," *Fibers Polym.*, vol. 19, no. 9, pp. 1813–1819, Sep. 2018, doi: 10.1007/s12221-018-8265-1.

- [73] R. Boni, A. Ali, A. Shavandi, and A. N. Clarkson, "Current and novel polymeric biomaterials for neural tissue engineering," *J. Biomed. Sci.*, vol. 25, no. 1, p. 90, Dec. 2018, doi: 10.1186/s12929-018-0491-8.
- [74] D. Arslantunali, T. Dursun, D. Yucel, N. Hasirci, and V. Hasirci, "Peripheral nerve conduits: technology update.," *Med. Devices Auckl. NZ*, vol. 7, pp. 405–424, 2014, doi: 10.2147/MDER.S59124.
- [75] Q. Zhang *et al.*, "Harnessing 3D collagen hydrogel-directed conversion of human GMSCs into SCP-like cells to generate functionalized nerve conduits," *Npj Regen. Med.*, vol. 6, no. 1, p. 59, Sep. 2021, doi: 10.1038/s41536-021-00170-y.
- [76] L. Ghasemi-Mobarakeh *et al.*, "Application of conductive polymers, scaffolds and electrical stimulation for nerve tissue engineering," *J. Tissue Eng. Regen. Med.*, vol. 5, no. 4, pp. e17–e35, Apr. 2011, doi: 10.1002/term.383.
- [77] A. M. El-hadi, "Biopolymer blend with semiconductivity for next generation in electronic devices," *Appl. Phys. A*, vol. 124, no. 6, p. 445, May 2018, doi: 10.1007/s00339-018-1846-4.
- [78] M. Li, Y. Guo, Y. Wei, A. G. MacDiarmid, and P. I. Lelkes, "Electrospinning polyaniline-contained gelatin nanofibers for tissue engineering applications," *Biomaterials*, vol. 27, no. 13, pp. 2705–2715, May 2006, doi: 10.1016/j.biomaterials.2005.11.037.
- [79] A. M. El-hadi, F. Y. Al-Jabri, and W. J. Altaf, "Higher dielectric properties of semiconducting biopolymer composites of poly(3-hydroxy butyrate) (PHB) with polyaniline (PANI), carbon black, and plasticizer," *Polym. Bull.*, vol. 75, no. 4, pp. 1681–1699, Apr. 2018, doi: 10.1007/s00289-017-2118-8.
- [80] A. M. El-hadi, A. M. Abd Elbary, and S. M. Alluqmani, "The role of polyaniline and plasticizer on the development of the electrical conductivity of PHB composites," *J. Compos. Mater.*, vol. 53, no. 16, pp. 2305–2314, Jul. 2019, doi: 10.1177/0021998319826348.
- [81] A. M. El-hadi and A. M. Abd Elbary, "Design of the electrically conductive PHB blends for biomedical applications," *J. Mater. Sci. Mater. Electron.*, vol. 29, no. 19, pp. 16496–16506, Oct. 2018, doi: 10.1007/s10854-018-9743-3.
- [82] J. P. Bothma, J. de Boor, U. Divakar, P. E. Schwenn, and P. Meredith, "Device-Quality Electrically Conducting Melanin Thin Films," *Adv. Mater.*, vol. 20, no. 18, pp. 3539–3542, Sep. 2008, doi: 10.1002/adma.200703141.
- [83] C. Giacomantonio, "Charge transport in melanin, a disordered bio-organic conductor," *Univ. Qld.*, 2005.
- [84] S. Cai, C. Wu, W. Yang, W. Liang, H. Yu, and L. Liu, "Recent advance in surface modification for regulating cell adhesion and behaviors," vol. 9, no. 1, pp. 971–989, 2020, doi: 10.1515/ntrev-2020-0076.

- [85] M. Gulino, D. Kim, S. Pané, S. D. Santos, and A. P. Pêgo, "Tissue Response to Neural Implants: The Use of Model Systems Toward New Design Solutions of Implantable Microelectrodes," *Front. Neurosci.*, vol. 13, 2019, [Online]. Available: <https://www.frontiersin.org/article/10.3389/fnins.2019.00689>
- [86] M. Barra *et al.*, "Eumelanin-based organic bioelectronics: myth or reality?," *MRS Adv.*, vol. 1, no. 57, pp. 3801–3810, 2016.
- [87] C. M. Murphy, M. G. Haugh, and F. J. O'Brien, "The effect of mean pore size on cell attachment, proliferation and migration in collagen–glycosaminoglycan scaffolds for bone tissue engineering," *Biomaterials*, vol. 31, no. 3, pp. 461–466, 2010.
- [88] F. J. O'Brien, B. A. Harley, I. V. Yannas, and L. J. Gibson, "The effect of pore size on cell adhesion in collagen-GAG scaffolds," *Biomaterials*, vol. 26, no. 4, pp. 433–441, 2005.
- [89] H. Amani *et al.*, "Controlling cell behavior through the design of biomaterial surfaces: a focus on surface modification techniques," *Adv. Mater. Interfaces*, vol. 6, no. 13, p. 1900572, 2019.
- [90] S. B. Kennedy, N. R. Washburn, C. G. Simon Jr, and E. J. Amis, "Combinatorial screen of the effect of surface energy on fibronectin-mediated osteoblast adhesion, spreading and proliferation," *Biomaterials*, vol. 27, no. 20, pp. 3817–3824, 2006.
- [91] J. Wei *et al.*, "Adhesion of mouse fibroblasts on hexamethyldisiloxane surfaces with wide range of wettability," *J. Biomed. Mater. Res. Part B Appl. Biomater. Off. J. Soc. Biomater. Jpn. Soc. Biomater. Aust. Soc. Biomater. Korean Soc. Biomater.*, vol. 81, no. 1, pp. 66–75, 2007.
- [92] S. Guo *et al.*, "Parallel control over surface charge and wettability using polyelectrolyte architecture: effect on protein adsorption and cell adhesion," *ACS Appl. Mater. Interfaces*, vol. 8, no. 44, pp. 30552–30563, 2016.
- [93] K. Tomaselli, P. Doherty, C. Emmett, C. Damsky, F. Walsh, and L. Reichardt, "Expression of beta 1 integrins in sensory neurons of the dorsal root ganglion and their functions in neurite outgrowth on two laminin isoforms," *J. Neurosci. Off. J. Soc. Neurosci.*, vol. 13, pp. 4880–8, Dec. 1993, doi: 10.1523/JNEUROSCI.13-11-04880.1993.
- [94] M. A. Arnaout, S. L. Goodman, and J.-P. Xiong, "Structure and mechanics of integrin-based cell adhesion," *Curr. Opin. Cell Biol.*, vol. 19, no. 5, pp. 495–507, 2007.
- [95] C. Pierret *et al.*, "Developmental cues and persistent neurogenic potential within an in vitro neural niche," *BMC Dev. Biol.*, vol. 10, no. 1, pp. 1–19, 2010.
- [96] W. Yang, H. Yu, G. Li, Y. Wang, and L. Liu, "Facile modulation of cell adhesion to a poly (ethylene glycol) diacrylate film with incorporation of polystyrene nano-spheres," *Biomed. Microdevices*, vol. 18, no. 6, pp. 1–9, 2016.

